tion, Madison, WI) or horseradish peroxidase conjugated anti-rabbit IgG antibody (Amersham Biosciences, Buckinghamshire, UK). Proteins were visualized by the alkaline phosphatase color reaction or by ECL system (Amersham Biosciences).

3. Results

3.1. Effect of IL-21 on IgE synthesis

We first investigated the effects of IL-21 on B-cell IgE synthesis in human PBMCs and highly purified human B cells. Apparent IgE synthesis was not recognized by PBMCs in the presence of medium alone, IL-4 alone, or IL-21 alone, but PBMCs produced detectable levels of IgE in the presence of IL-4 plus CD40 mAb or IL-4 plus CD40 mAb/CD32T, which further strengthen CD40 signaling more than that with CD40 mAb alone. IL-21 did not enable the detectable levels of IgE production in the presence of IL-4 alone but marginally elevated IgE production with IL-4 plus CD40 mAb. Notably, IL-21 markedly enhanced IgE production in the presence of IL-4 plus CD40 mAb/CD32T ($p < 0.005$, one-tailed paired t test, $n = 12$) (Figure 1A).

As reported previously (7), IL-10 also enhanced IgE synthesis in the presence of IL-4 plus CD40 mAb/CD32T, and IL-10 and IL-21 further enhanced the synthesis of IgE under these conditions ($p < 0.005$, a one-tailed paired t test, $n = 12$) (Figure 1A). To exclude the effect of T cell and monocyte contamination, we also examined IgE synthesis of B cells that were purified by negative selection. Similarly to PBMCs, IL-21 remarkably enhanced the production of IgE especially in the presence of IL-4 plus CD40 mAb/CD32T ($p < 0.05$, a one-tailed paired t-test, $n = 5$) or IL-4 plus CD40 mAb/CD32T plus IL-10 ($p < 0.005$, a one-tailed paired t test, $n = 5$) (Figure 1B). The enhancement of IgE synthesis by IL-21 was found in both of naïve and memory B cells (Figure 2).

3.2. Effect of IL-21 on expression of germline ε and AID transcripts

The induction of germline ε transcripts is an early process in IgE synthesis and is necessary for IgE production. We therefore investigated whether IL-21 promotes the induction of germline ε transcripts. Germline ε transcripts were slightly detectable in purified B cells cultured with medium alone, and were enhanced with IL-4 plus CD40 mAb but were unaffected in cells incubated in addition with IL-21 (Figure 3A). However, IL-21 remarkably enhanced AID mRNA expression in the presence of IL-4, CD40 mAb (data not shown), or both (Fig. 3B). These findings suggest that the enhancement of IgE production by IL-21 does not depend on the induction of germline ε transcripts, but might depend on the enhancement of AID synthesis.

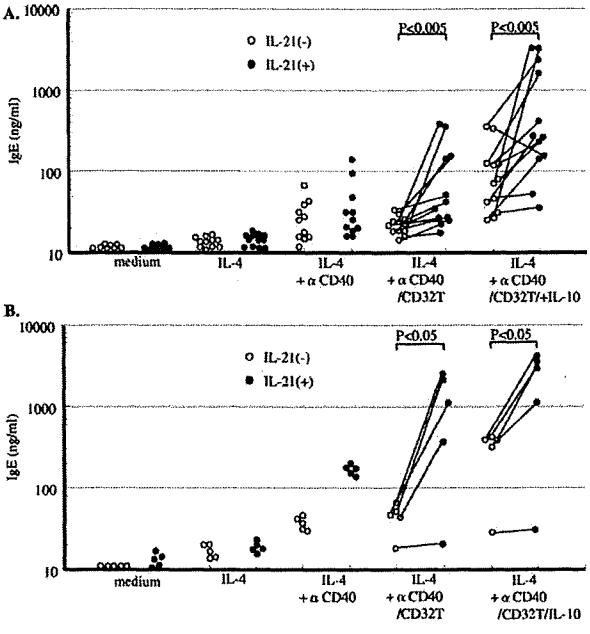

Fig 1. Enhancement of IgE synthesis by IL-21. (A) PBMCs ($n = 12$) or (B) highly purified human B cells ($n = 5$) obtained by negative selection were cultured with IL-4, IL-4 plus ant-CD40, IL-4 plus anti-CD40 /CD32T, or IL-4 plus anti-CD40/CD32T plus IL-10 with or without IL-21 at a final cell density of 5–10 ×105 cells/ml in a volume of 200 μl/well. After 12–14 days, supernatants were harvested and IgE content was measured by ELISA. Statistics were performed using the paired t test.

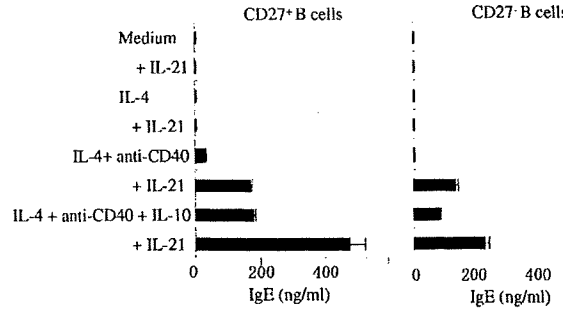

Fig 2. Production of IgE by naïve and memory B cells. $CD20^+CD27^-$ or $CD20^+CD27^+$ B cells were isolated from the PBMNCs by means of flow cytometry (purity was ≥98%, respectively). Highly purified B cells were incubated with indicated stimuli for 12 days. IgE content was measured by ELISA. Results are expressed as the mean ± SD of triplicate determinations. A similar result was obtained in another experiment.

3.3. Generation of plasma cells by IL-21

Because the differentiation of B cells into plasma cells is crucial for IgE production, we studied the effects of IL-21 on purified human B-cell differentiation in the presence of IL-4 or IL-4 plus CD40 mAb/CD32T. Generally, human B cells express a high level of CD 20 and a low level of CD38, and plasma cells express a high level of CD 38 (CD38hi). Flow-cytometric analysis revealed that IL-21 induced a marginal increase in the number of plasma cells after 12–14 days of B-cell culture. Plasma cells were remarkably increased by IL-21 especially in the presence of IL-4 plus CD40 mAb/CD32T (Fig. 4A). To further demonstrate that CD38hi cells are indeed producing IgE, intracellular staining for IgE in CD38hi cells in these cultures were performed. As shown in Figure 4B, a portion of CD38hi cells contained a large amount of IgE in the cytoplasm. These results demonstrate that IL-21 promotes the generation of IgE-producing plasma cells in the presence of stimuli.

3.4. Expression of Blimp-1 and XBP-1 by IL-21

Blimp-1 and XBP-1 are known critical genes for plasma cell differentiation. To further clarify the mechanism of plasma cell differentiation by IL-21, we examined the expression of Blimp-1 and XBP-1 in purified human B cells. Because expression of Blimp-1 and XBP-1 peaked at a maximum level at day 2 to 3 of culture (data not shown), B cells were cultured for 3 days. The expression of XBP-1 mRNA in B cells was not enhanced with IL-21 signaling with or without IL-4, or IL-4 plus CD40 mAb, respectively (Fig. 4C). Western blot analysis also showed that IL-21 did not induce the expression of XBP-1 at the protein levels (Fig. 4D). However, IL-21 signaling enhanced the expression of Blimp-1 at the mRNA levels (Fig. 4C), indicating that the differentiation of human B cells into plasma cells by IL-21 is strongly associated with the expression of Blimp-1.

4. Discussion

During humoral B cell-dependent immune systems, a variety of cytokines and co-stimulators regulate B-cell functions. This study

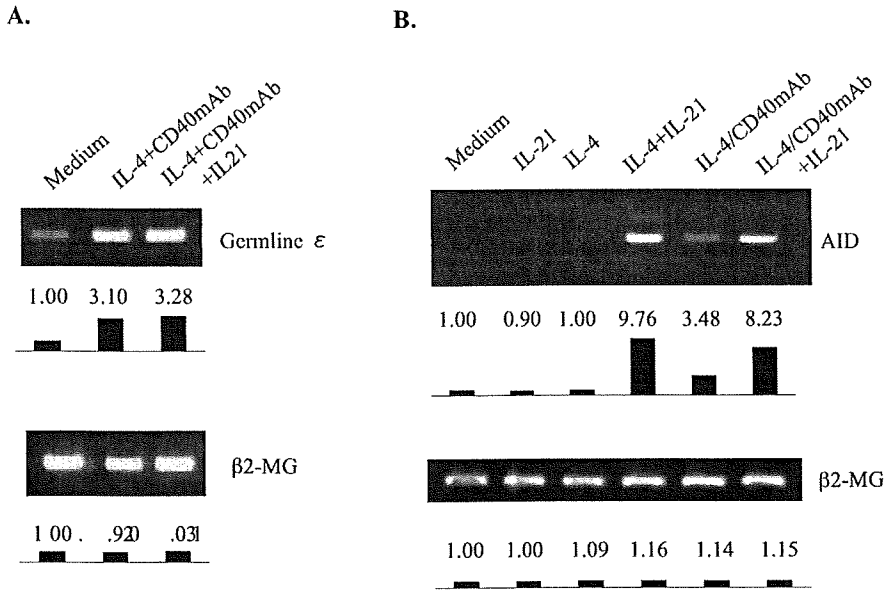

Fig 3. Germline ε expression and AID mRNA expression by IL-21. Highly purified human B cells were stimulated as indicated, cultured and harvested. Each template contained the same amount of mRNA extracted from 2 × 106 B cells. The mRNA expression of germline ε (A) and AID (B) were determined using RT-PCR analysis with β2-MG as a control. The-fold induction based on medium alone as 1.00 is shown below each band.

demonstrates that IL-21 is an important promoter of plasma cell differentiation by enhancing Blimp-1 mRNA expression, subsequently IL-21 strongly stimulates IgE production in humans. Although the effects of IL-21 on IgE have been widely reported, there have been several discrepancies among papers in the context of IL-21-induced IgE production. Previous studies in mice have shown IL-21 to be an essential factor in the generation of plasma cells [12], and another report has tied IL-21 to B-cell immunoglobulin synthe-

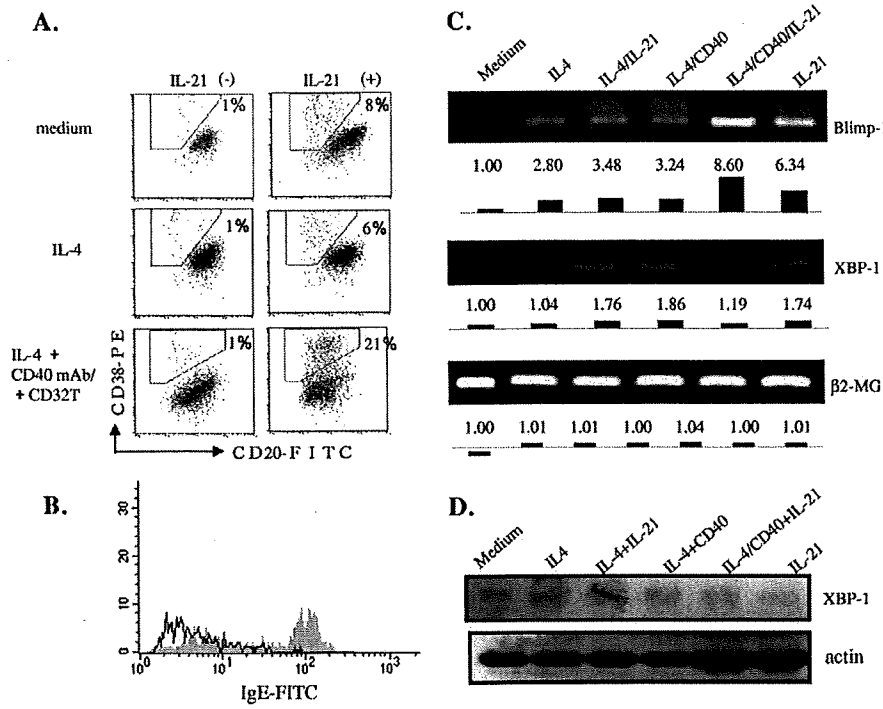

Fig 4. Effects of IL-21 signaling on differentiation to plasma cells and transcripts of Blimp-1. (A) Highly purified human B cells were cultured with medium alone, IL-4, or IL-4 plus anti-CD40/CD32T with or without IL-21, respectively, for 12–14 days. Cells were then stained with anti-CD20-FITC and anti-CD38-PE and evaluated by flow-cytometric analysis. The fraction of CD20lowCD38high cells is considered to be a plasma cell population. (B) Purified human B were cultured with IL-4 plus anti-CD40 plus IL-21 for 7days. After permealizing membranes, the cells were stained with anti-IgE (4.15) after goat anti-mouse Ig-FITC and anti-CD38-PE. Histogram data indicating the fluorescence intensity are displayed with FITC for IgE (closed histogram) and the isotype negative control (open histogram) gated on CD38hi cells. (C) Purified human B cells were cultured with medium alone, IL-4, or IL-4 plus anti-CD40 with or without IL-21, respectively, for 2 days. After extraction of total mRNA from cultured 2 × 106 B cells, RT-PCR analysis was performed with β2-MG as a control. The-fold induction is shown directly below each band. (D) Human B cells were stimulated with indicated stimuli for 5 days. Whole cell lysates were analyzed by Western blotting with antibodies to XBP-1 and β-actin. The data shown are representative of those from two independent experiments.

ses [20], suggesting that IL-21 factors crucially in the Ig secretion of B cells and differentiation into plasma cells in both humans and mice. In murine systems, IL-21 induces Ig isotype switching but inhibits IgE production. Suto *et al.* examined the effect of IL-21 on antigen-specific IgE production in mice, and found that down-regulation of IgE production is induced by inhibition of IL-4 dependent isotype switching to IgE at the level of germline ε transcription [13]. As regarding effects of IL-21 in human systems, Caven *et al.* reported that IL-21–dependent IgE production in *in vitro* culture systems in humans and mice is cell density and cell division dependent and is augmented by IL-10 [14]. They also demonstrated that B-cell receptor ligation antagonizes the enhancement of anti-CD40 / IL-4 induced plasma cell differentiation by IL-21, and increased IgE production is seen in low cell densities when IL-21 is added to human B-cell cultures activated with anti-CD40 /IL-4 [21]. Wood *et al.* indicated that IL-21 induced IL-4 driven IgE synthesis by mitogen-stimulated human PBMCs [22].

The processes of IgE production by B cells involves IgE class switching, clonal expansion of B cells, and differentiation into IgE-secreting plasma cells [1]. AID is the only B cell-specific component that is necessary and sufficient for both CSR and somatic hypermutation [23]. We observed that IL-21 remarkably enhanced AID mRNA expression in the presence of IL-4, anti-CD40 (data not shown), or both of them. These findings suggest that the enhancement of IgE production by IL-21 depends on, at least some part, the enhancement of AID expression. The differentiation of B cells into plasma cells is also crucial for IgE production.

Flow-cytometric analysis revealed that IL-21 induced an increase in the number of plasma cells after 12–14 days of B-cell culture especially upon IL-4 with anti-CD40 /CD32T. Blimp-1 and XBP-1 are known critical genes for plasma cell differentiation. We further clarified the mechanism of plasma cell differentiation by IL-21, and found that the differentiation of human B cells into plasma cells by IL-21 is strongly associated with the expression of Blimp-1 by semi-quantitative RT-PCR. However, regarding effects of IL-4 or IL-21 on plasma cell differentiation, some aspects are still a matter of debate in humans. Interestingly, Ettinger *et al.* demonstrated that IL-4 inhibited IL-21–induced plasma cell differentiation [24]. However, percentage of plasma cells was 3% in the presence of anti-CD40/IL-21 and 5% in anti-CD40/IL-21/IL-4, and the addition of IL-4 greatly diminished plasma cell differentiation upon BCR cross-linkage in addition to anti-CD40/IL-21, indicating BCR signaling has much effect on the inhibition mediated by IL-4 [24]. Ettinger *et al.* also reported that IL-4 mildly inhibited Blimp-1 mRNA expression in the presence of anti-CD40/IL-21, and IL-4 greatly inhibited Blimp-1expressin upon anti-CD40/BCR cross-linkage with anti-IgM mAb/IL-2/IL-21 [24], suggesting that the inhibition by IL-4 gets involved with BCR signaling. Our findings that stimulation with anti-CD40/IL-4/IL-21 resulted in the greatest frequency of plasma-like cells, contrast that published by Ettinger *et al.* and Bryant *et al.* that IL-4 suppressed IL-21-induced generation of plasma cells [15,24]. In marked contrast, Caven *et al.* revealed the extreme increase of plasma cells by IL-21 in the presence of IL-4/anti-CD40 [14]. Bryant *et al.* [15] reported IL-4 inhibited Blimp-1 expression by naive B cells upon CD40L/IL-21, but not by memory B cells. However, because Blimp-1 expression in these investigators' experiment was prominent in memory B cells, there could not be a difference about Blimp-1 expression with or without IL-4 in total B cells. In regard to XBP-1 expression, there is also the difference between our finding that IL-21 did not increase XBP-1 and another reported finding. Caven *et al.* reported that B cells differentiated into plasma cells with increased expression of XBP-1 when stimulated with anti-CD40/IL-4/IL-21[21]. However, XBP-1 transcription was increased at low cell numbers of culture by the addition of IL-21, whereas no enhancement of XBP-1 transcription was occurring at usual cell concentration in their system. The finding is consistent with our finding with using usual concentrations of cell numbers cultured. Meanwhile, Pene *et al.* revealed that IL-21 differentially regulates IL-4-induced human IgE production by various conditions such as IL-21 concentrations, donor variation and IFN-γ production in the culture system [16]. The reason of the above discrepancies is not clear. The difference of B-cell concentrations, IL-21 concentrations, donor variation, effect of IFN-γ, or the strength of CD40 signaling may develop the different results.

IL-21 is a pleiotrophic cytokine with effects on T, B, and NK cells. During of the humoral B-cell immune response in mice, IL-21 has been found to have conflicting functions [25]; in the absence of signaling through BCR, IL-21 induces apoptosis of B cells, but in the presence of signaling through the BCR, IL-21 induces CSR and Ig production, together with differentiation of B cells towards plasma cells. These findings reveal that IL-21 might help to eliminate B cells responsible for nonspecific hyperglobulinemia. Interestingly, we observed that IL-21 induces dramatically IgE production by human B cells by means of double stimulation mechanism; CSR by AID expression and B-cell terminal differentiation through Blimp-1 expression. However, it is unclear why IL-21, which has the common promotional effect to B-cell terminal differentiation, induces the different agency on the production of IgE between humans and mice.

In summary, IL-21 increases IgE synthesis concomitantly with AID expression and promotes differentiation into plasma cells via Blimp-1. This study has elucidated one of the functions of IL-21in B-cell immune response in human beings. These findings may provide insights into future therapeutic studies of allergic disease.

Acknowledgments

We thank W.P. Meun for photography, M. Kleijer for technical assistance, and Dr. R.A.W. van Lier and R. Hoogeboom for critical reading of the manuscript. We thank Yumiko Negishi (student at Shnishu University, Matsumoto, Japan), Drs. Kazuko Yamazaki and Takashi Yamazaki for their technical assistance, and Susumu Ito for sorting the cells.

References

[1] Geha RS, Jabara HH, Brodeur SR. The regulation of immunoglobulin E class-switch recombination. Nat Rev Immunol 2003;3:721–32.
[2] de Vries JE, Punnonen J, Cocks BG., de Waal Malefyt R, Aversa G. Regulation of the human IgE response by IL4 and IL13. Res Immunol 1993;144:597–601.
[3] Muramatsu M, Kinoshita K, Fagarasan S, Yamada S, Shinkai Y, Honjo T. Class switch recombination and hypermutation require activation-induced cytidine deaminase (AID), a potential RNA editing enzyme. Cell 2000;102:553–63.
[4] Revy P, Muto T, Levy Y, Geissmann F, Plebani A, Sanal O, et al. Activation-induced cytidine deaminase (AID) deficiency causes the autosomal recessive form of the hyper-IgM syndrome (HIGM2). Cell 2000;102:565–75.
[5] Turner CA, Jr, Mack DH, Davis MM. Blimp-1, a novel zinc finger-containing protein hat can drive the maturation of B lymphocytes into immunoglobulin-secreting cells. Cell 1994;77:297–306.
[6] Reimold AM, Iwakoshi NN, Manis J, Vallabhajosyula P, Szomolanyi-Tsuda E, Gravallese EM, et al. Plasma cell differentiation requires the transcription factor XBP-1. Nature 2001;412:300–7.
[7] Kobayashi N, Nagumo H, Agematsu K. IL-10 enhances B-cell IgE synthesis by promoting differentiation into plasma cells, a process that is inhibited by CD27/CD70 interaction. Clin Exp Immunol 2002;129:446–52.
[8] Yssel H, Abbal C, Pène J, Bousquet J. The role of IgE in asthma. Clin Exp Allergy 1998;28:104–9.
[9] Xu L, Rothman P. IFN-gamma represses epsilon germline transcription and subsequently down-regulates switch recombination to epsilon. Int Immunol. 1994;6:515–21.
[10] Parrish-Novak J, Dillon SR, Nelson A, Hammond A, Sprecher C, Gross JA, et al. Interleukin 21 and its receptor are involved in NK cell expansion and regulation of lymphocyte function. Nature 2000;408:57–63.
[11] Coquet JM, Kyparissoudis K, Pellicci DG, Besra G, Berzins SP, Smyth MJ, Godfrey DI. IL-21 is produced by NKT cells and modulates NKT cell activation and cytokine production. J Immunol 2007;178:2827–34.
[12] Ozaki K, Spolski R, Feng C. G, Qi C. F, Cheng J, Sher A, A critical role for IL-21 in regulating immunoglobulin production. Science. 2002;298:630–4.
[13] Suto A, Nakajima H, Hirose K, Suzuki K, Kagami S, Seto Y. Interleukin 21 prevents antigen-induced IgE production by inhibiting germ line epsilon transcription of IL-4-stimulated B cells. Blood 2002;100:4565–73.
[14] Caven TH, Shelburne A, Sato J, Chan-Li Y, Becker S, Conrad DH. IL-21 dependent IgE production in human and mouse in vitro culture systems is cell density and

cell division dependent and is augmented by IL-10. Cell Immunol 2005;238:123-34.
[15] Bryant VL, Ma CS, Avery DT, Li Y, Good KL, Corcoran LM, de Waal Malefyt R, Tangye SG. Cytokine-mediated regulation of human B-cell differentiation into Ig-secreting cells: Predominant role of IL-21 produced by $CXCR5^{+/-}$ T follicular helper cells. J Immunol 2007;179:8180-90.
[16] Pène J, Guglielmi L, Gauchat JF, Harrer N, Woisetschläger M, Boulay V, Fabre JM, Demoly P, Yssel H. IFN-gamma-mediated inhibition of human IgE synthesis by IL-21 is associated with a polymorphism in the IL-21R gene. J Immunol 2006; 177:5006-13.
[17] Chomczynski P, Sacchi N. Single-step method of RNA isolation by acid guanidinium thiocyanate-phenol-chloroform extraction. Anal Biochem 1987;162: 156-9.
[18] Karasuyama H, Kudo A, Melchers F. The proteins encoded by the VpreB and lambda 5 pre-B cell-specific genes can associate with each other and with mu heavy chain. J Exp Med 1990;172:969-72.
[19] Streuli M, Morimoto C, Schrieber M, Schlossman SF, Saito H. Characterization of CD45 and CD45R monoclonal antibodies using transfected mouse cell lines that express individual human leukocyte common antigens. J Immunol. 1988;141:3910-4.
[20] Ozaki K, Spolski R, Ettinger R, Kim HP, Wang G, Qi CF, et al. Regulation of B cell differentiation and plasma cell generation by IL-21, a novel inducer of Blimp-1 and Bcl-6. J Immunol 2004;173:5361-71.
[21] Caven TH, Sturgill JL, Conrad DH. BCR ligation antagonizes the IL-21 enhancement of anti-CD40/IL-4 plasma cell differentiation and IgE production found in low density human B cell cultures. Cell Immunol 2007;247:49-58.
[22] Wood N, Bourque K, Donaldson DD, Collins M, Vercelli D, Goldman SJ, et al. IL-21 effects on human IgE production in response to IL-4 or IL-13. Cell Immunol 2004;231:133-45.
[23] Notarangelo LD, Lanzi G, Peron S, Durandy A. Defects of class-switch recombination. J Allergy Clin Immunol 2006;117:855-64.
[24] Ettinger R, Sims GP, Fairhurst AM, Robbins R, da Silva YS, Spolski R, et al. IL-21 induces differentiation of human naive and memory B cells into antibody-secreting plasma cells. J Immunol 2005;175:7867-79.
[25] Mehta DS, Wurster AL, Whitters MJ, Young DA, Collins M, Grusby MJ. IL-21 induces the apoptosis of resting and activated primary B cells. J Immunol 2003;170:4111-8.

Structural basis for the multiple interactions of the MyD88 TIR domain in TLR4 signaling

Hidenori Ohnishi[a], Hidehito Tochio[b,1], Zenichiro Kato[a,c,d,1], Kenji E. Orii[a], Ailian Li[a], Takeshi Kimura[a], Hidekazu Hiroaki[e], Naomi Kondo[a,c,d], and Masahiro Shirakawa[b,f]

[a]Department of Pediatrics, Graduate School of Medicine, [c]Center for Emerging Infectious Diseases, and [d]Center for Advanced Drug Research, Gifu University, Gifu, 501-1194, Japan; [b]Department of Molecular Engineering, Graduate School of Engineering, Kyoto University, Kyoto, 615-8510, Japan; [e]Division of Structural Biology, Graduate School of Medicine, Kobe University, 7-5-1, Kusunoki-cho, Chuo-ku, Kobe, Hyogo, 650-0017, Japan; and [f]Core Research for Evolutional Science and Technology, Japan Science and Technology Corporation, Hon-cho 4-1-8, Kawaguchi, Saitama, 332-0012, Japan

Edited by Jack L. Strominger, Harvard University, Cambridge, MA, and approved April 29, 2009 (received for review December 19, 2008)

Myeloid differentiating factor 88 (MyD88) and MyD88 adaptor-like (Mal) are adaptor molecules critically involved in the Toll-like receptor (TLR) 4 signaling pathway. While Mal has been proposed to serve as a membrane-sorting adaptor, MyD88 mediates signal transduction from activated TLR4 to downstream components. The Toll/Interleukin-1 receptor (TIR) domain of MyD88 is responsible for sorting and signaling via direct or indirect TIR–TIR interactions between Mal and TLR4. However, the molecular mechanisms involved in multiple interactions of the TIR domain remain unclear. The present study describes the solution structure of the MyD88 TIR domain. Reporter gene assays revealed that 3 discrete surface sites in the TIR domain of MyD88 are important for TLR4 signaling. Two of these sites were shown to mediate direct binding to the TIR domain of Mal. Interestingly, Mal-TIR, but not MyD88-TIR, directly binds to the cytosolic TIR domain of TLR4. These observations suggested that the heteromeric assembly of TIR domains of the receptor and adaptors constitutes the initial step of TLR4 intracellular signal transduction.

docking simulation | Mal | innate immunity | NMR | protein structure

Myeloid differentiating factor 88 (MyD88) is a cytosolic adaptor protein that plays essential roles in both innate and acquired immune responses by mediating signal transduction pathways that are initiated by Toll-like receptors (TLRs) and IL-1 and IL-18 receptors (IL-1R and IL-18R). MyD88 consists of an N-terminal death domain (DD) (approximately 90 aa residues), a C-terminal Toll/Interleukin-1 receptor (TIR) domain (approximately 150 aa residues), and a short connecting linker (1). In innate immune responses, the TIR domain of MyD88 has pivotal functions in the formation of signal initiation complexes involving the cytosolic domain of TLRs. The best characterized pathway is the TLR4 pathway, in which the cytosolic TIR domain of LPS-stimulated TLR4 interacts with the TIR domain of MyD88 (MyD88-TIR), in cooperation with another TIR-containing adaptor protein, MyD88 adaptor-like (Mal). Subsequently, signal is transmitted to the IL-1 receptor-associated kinase (IRAK) through an interaction between the death domains of MyD88 and IRAK. This eventually activates the transcription factors NF-κB and activator protein 1 (AP-1) via a phosphorylation cascade (2).

MyD88 has been reported to be involved in signaling pathways initiated by all TLRs thus far reported, with the exception of TLR3 (3). Of the MyD88-dependent pathways involving TLR2, 4, 5, 7, and 9, only the TLR2 and TLR4 pathways require Mal for efficient signal transduction (4). TLR4 also possesses the MyD88-independent signaling pathway, which comprises other TIR-containing cytosolic adaptors, TIR domain-containing adaptor inducing IFN-β (TRIF), TRIF-related adaptor molecule (TRAM), and sterile α and huntingtin-elongation-A subunit-TOR (HEAT) Armadillo motifs (SARM) (5). Therefore, in general, specific complexes involving more than one TIR-containing adaptor are likely to be required for initiation of each TLR signal transduction pathway.

Recently, Kagan and Medzhitov (6) revealed that MyD88 and Mal have distinctly different roles in TLR4 signaling: MyD88 serves as an essential "signaling adaptor," which transmits signals from ligand-activated TLRs to downstream factors to initiate kinase-dependent signaling cascades, while Mal functions as a "sorting adaptor," which recruits MyD88 to the plasma membrane via its PIP2 binding domain to promote interaction between MyD88 and activated TLR4 beneath the membrane. Indeed, Mal was shown to be dispensable for TLR4 signaling when MyD88 is fused to a PIP2 targeting domain. In the TLR4-TRIF pathway, TRAM has been proposed to serve as a sorting adaptor, which delivers TRIF to a specific membrane portion via its myristoylation site (7). These findings suggest that specific combinations of "sorting" and "signaling" TIR-containing adaptors might be involved in TLR signaling pathways.

The specificities of TIR–TIR interactions between adaptors, and between adaptors and TLRs, define the formation of various complexes that initiate TLR signaling pathways. However, little is known about the mechanism of heteromeric interactions between TIR domains. The crystal structures of cytosolic TIR domains of the membranous receptors, TLR1, TLR2, TLR10, and IL-1RAPL have been reported (8–10), and the homomeric TIR interfaces observed in the crystals have been described. However, the functional relevance of these homomeric interactions remains obscure because the formation of a homomeric dimer in these TIR domains has not been observed in solution (9, 10). Based on crystal structures and mutational data, several structural models have been proposed for heteromeric TIR–TIR interactions, which commonly suggest the importance of the so-called BB loop in these interactions (11, 12).

The present study describes the solution structure of MyD88-TIR using NMR spectroscopy. The isolated domain was shown to exist as a monomer in solution state on the basis of size-exclusion chromatography, although full-length MyD88 forms a dimer, which appears to be mediated via homomeric interactions within its death domain. By combining in vitro mutational binding experiments with an NF-κB reporter system in mammalian cells, 2 surface sites were identified as binding interfaces for the TIR domain of the sorting adaptor Mal, one of which includes a critical residue for MyD88 function, whose mutation causes the pyogenic bacterial infections

Author contributions: H.O., H.T., Z.K., N.K., and M.S. designed research; H.O., H.T., Z.K., K.E.O., A.L., T.K., and H.H. performed research; H.O., H.T., Z.K., and M.S. analyzed data; and H.O., H.T., Z.K., and M.S. wrote the paper.

The authors declare no conflict of interest.

This article is a PNAS Direct Submission.

Freely available online through the PNAS open access option.

Data deposition: The atomic coordinates have been deposited in the Protein Data Bank, www.pdb.org (PDB ID code 2Z5V).

[1]To whom correspondence may be addressed. E-mail: tochio@moleng.kyoto-u.ac.jp or zen-k@gifu-u.ac.jp.

This article contains supporting information online at www.pnas.org/cgi/content/full/0812956106/DCSupplemental.

www.pnas.org/cgi/doi/10.1073/pnas.0812956106

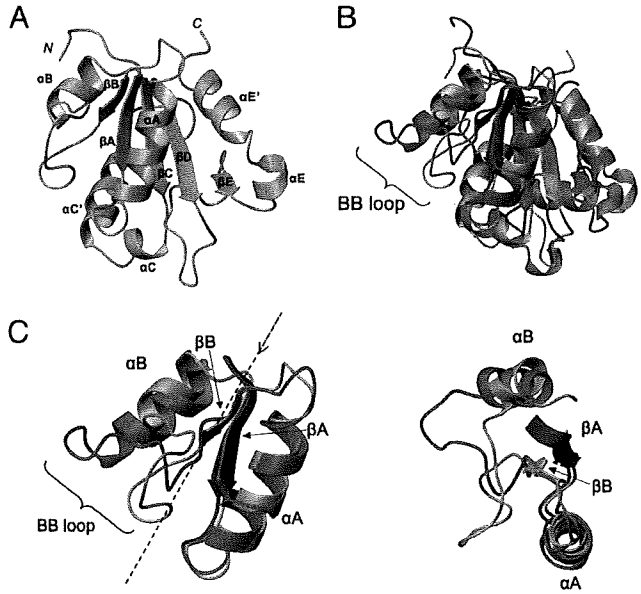

Fig. 1. Solution structure of the TIR domain of human MyD88. (*A*) A representative ribbon drawing of the NMR structure of MyD88, generated with MOLMOL 2K.2. The notation of the secondary structures (βA-βE, αA-αC, and αE) is based on TLR TIR domains. (*B* and *C*) A superimposed representation of MyD88-TIR (sky blue) and the crystal structure of the TIR domain of TLR2 (orange). Although the β-sheet cores are similar (rmsd = 0.90 Å), there are differences in some regions.

(13). Furthermore, the in vitro binding experiments demonstrated that MyD88-TIR does not directly bind to the cytosolic TIR domain of TLR4, while Mal-TIR does. The distal location of the Mal binding sites on the MyD88-TIR surface suggests that the TIR domain of MyD88 simultaneously interacts with 2 Mal-TIR molecules, which may provide a highly efficient scaffold for signal transduction.

Results

Structure Determination of the TIR Domain of MyD88. Based on sequence comparison between TIR domains, a region was selected that comprised residues 148–296 of human MyD88 and was used for structure determination by solution NMR spectroscopy (see Fig. S1). In the buffer used for structural studies, MyD88-TIR resided in a monomeric state, as assumed from size-exclusion chromatography. However, the death domain including internal domain (DD+ID) of MyD88 existed in a dimeric state (see Fig. S2). Therefore, the reported MyD88 dimerization was likely mediated by DD+ID but not by the TIR domain (14). The TIR domain structure of human MyD88 (residues 157–296), which presented the lowest overall energies in the 20 final structures generated by calculations, is shown in Fig. 1*A*. Statistics for the final 20 conformers are summarized in Table S1, which shows that the rmsd for the coordinates of backbone heavy atoms (N, Cα, and C') of residues 157–185, 188–194, and 203–295 is 0.45 Å. The N-terminal 9 residues (148–156) displayed random coil propensity, which was characterized by the lack of medium-to-long range NOESY cross-peaks for the region. Hence, these residues were omitted from the figure and statistics for clarity.

Previous studies have indicated that 3 short, sequence motifs, called box 1–3 motifs, which are (F/Y)DA, RDXXPG, and FW, respectively, are conserved between TIR domains (see Fig. S1) (15). Of these, the box 2 motif, which resides in the so-called BB loop region, has been suggested to be important for TIR–TIR interactions and specificities (8, 16). In the calculated conformers of MyD88-TIR, a section of the BB loop, namely residues 194–208, was not well converged. With the exception of Gly-201, Val-204, and Ser-206, the backbone amide resonances of these residues were not identified in 2D ^{1}H-^{15}N hetero-nuclear single quantum coherence (HSQC) spectra, although resonances of some side chain protons were observed and assigned in HCCH-TOCSY and 3D ^{13}C-edited NOESY spectra. This region appeared to not form a single, definite structure, as judged from observations of a relatively few number of long-range NOEs. A $\{^{1}H\}$-^{15}N heteronuclear NOE experiment showed that some main-chain amide groups in the BB loop region, namely Gly-201, Val-204, and Ser-206, displayed NOE values of 0.67, 0.55, and 0.67, respectively, which were less than the average value for residues 157–297 (0.76 ± 0.09). These results implied that the BB loop was mobile in solution. The presumed conformational flexibility in the BB loop region might exert broadening effects due to chemical exchange, which results in absence of the backbone amide resonances of residues 195–200, 202, and 203. In addition, the turn region comprising residues 185–188, which follows helix αA, was poorly defined as the main chain amide resonances of Thr-185, Asp-186, Tyr-187, and Arg-188 could not be identified in the HSQC spectrum.

During the preparation of this manuscript, Rossi et al. released the solution structure of the TIR domain of human MyD88 in the Protein Data Bank (PDB ID: 2JS7). The overall folding was identical to our findings, despite minor differences. However, a detailed comparison of these 2 structures would not be appropriate, because of substantial differences in solution conditions, such as organic additives and pH. The structure of Rossi et al. was determined in a buffer containing 5% acetonitrile at pH 5.0, while the present structure determination was performed in a buffer at pH 6, with no organic solvent.

Structural Description of the TIR Domain of MyD88, and Comparison with Other TIR Domains. The MyD88 TIR domain structure (residues 157–296) comprised a central 5-stranded parallel β-sheet (βA–βE) surrounded by 4 α-helices (αA–αC and αE) (Fig. 1*A*). As predicted, the global fold was similar to what was observed in previously determined crystal structures of TIR domains of receptors TLR1, TLR2, TLR10, and IL-1RAPL (PDB codes: 1FYV, 1FYW, 2J67, and 1T3G, respectively). Of the known structures, the MyD88 TIR domain exhibited highest sequence similarity to TLR2. Fig. 1 *B* and *C* show superimposed representations of the TIR domain structures from MyD88 and TLR2. While the β-sheet cores displayed high structural similarity, as indicated by an rmsd value for backbone N, Cα, and C' of 0.90 Å, several regions displayed notable conformational differences. The largest structural discrepancy was observed in the region from the BB loop (Ser-194–Ala-208 of the MyD88 TIR domain) to αB (Fig. 1*C*). The BB loop was exposed to solvent in MyD88 and TLR2, but the direction in which the loops orient was markedly different. This was mainly due to a structural difference in the C-terminal region of the BB loop (residues 205–208), which precedes αB of MyD88. These residues adopted an extended conformation in MyD88, whereas corresponding residues are involved in an α-helix (αB) in TLR2. Therefore, αB of MyD88 was much shorter than TLR2. Another major conformational difference was the lack of an α-helix in the region between strands βD and βE (residues 257–273) of the MyD88 TIR domain (see Fig. S1). This region adopted an extended and a short helical coil conformation in MyD88, but the corresponding residues formed an α-helix (αD) in TLR2 (positions 266–270 in MyD88 numbering).

Cell-Based Functional Assays of the MyD88 TIR Domain in TLR4 Signaling Pathways. To explore residues that are important for function of the MyD88 TIR domain, we performed mutational analysis of the domain, using dominant negative effects of ectopically expressed isolated TIR domain (17). For the assay, a luciferase reporter system for NF-κB activation was constructed in HEK293 cells, where MyD88-TIR or mutants harboring single amino acid substitutions of surface residues, was ectopically expressed. Expression of

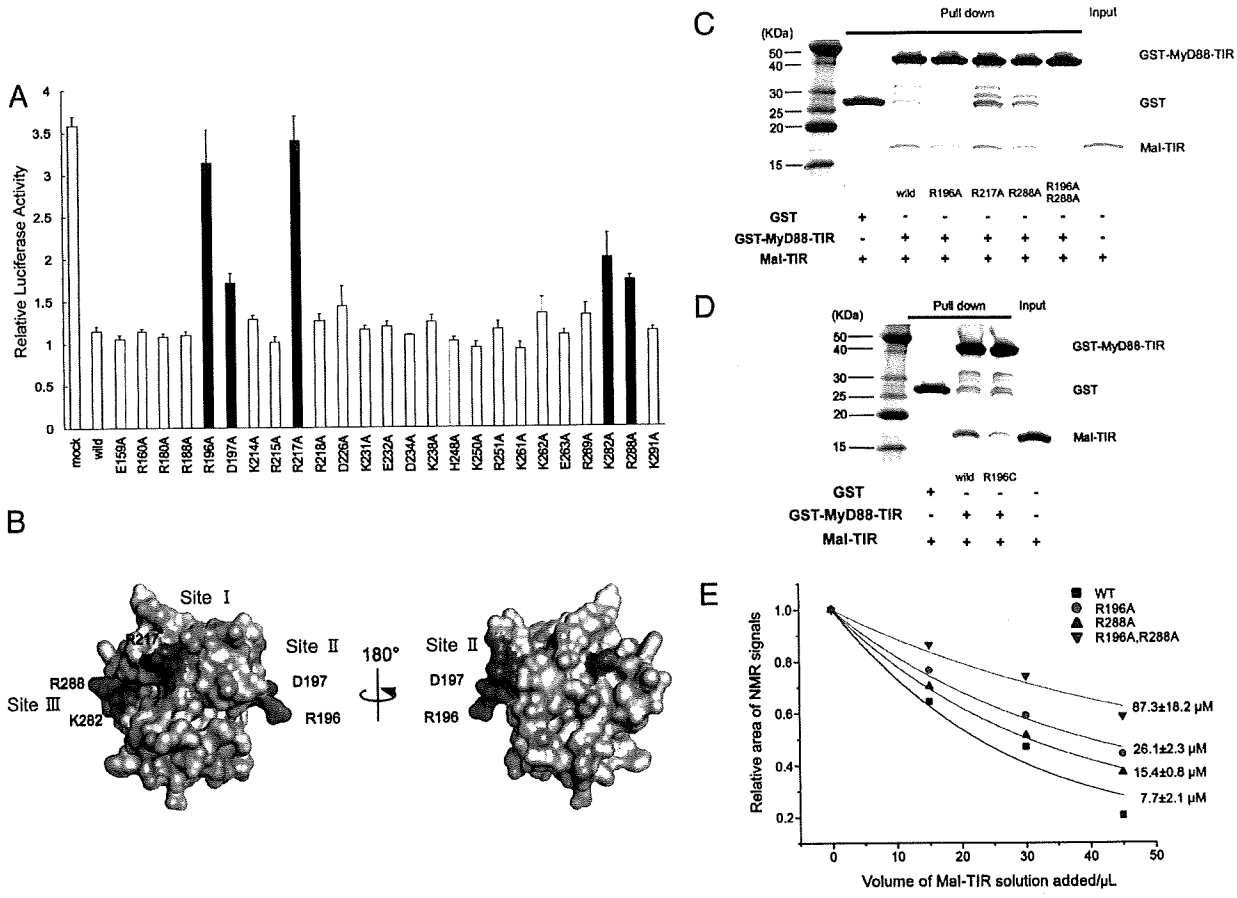

Fig. 2. Functional sites for signaling and binding sites for Mal. (*A*) The NF-κB reporter gene assay of MD2 cotransfected with LPS-induced (1.0 μg/ml) 293-hTLR4A-HA cells. In these graphs, each column indicates relative luciferase activity of stimulated cells over nonstimulated cells. Color code: black bars indicate a significant increased NF-κB activity, compared with the wild-type group. The statistical significance of differences in luciferase activities between wild type and mutants was analyzed using the Dunnett's multiple comparison test. Statistical significance was assumed to be $P < 0.05$. (*B*) Results of the functional assays of LPS/TLR4 signaling presented on the 3D structure of the TIR domain of MyD88. The results of the functional assays are mapped onto the molecular surface of the MyD88 TIR domain. The amino acid residues judged to be significant by the luciferase assay are shown in red, while nonsignificant residues are shown in light brown. The conserved motifs of boxes 1–3 (FDA of box1, VLPG of box2, FW of box3) are shown in blue. (*C*) Assay of binding of Mal TIR domain and MyD88 TIR domain wild type or mutants. Alanine substitutions in Site II (R196A) or Site III (R288A) in MyD88 resulted in reduced interaction with Mal. The double alanine substituted mutant of Site II and Site III caused complete abolition of the interaction with Mal. (*D*) Cysteine substitution in R196 also caused reduced interaction with Mal. (*E*) Plots of relative integrated area of NMR signals, which were derived from NMR titration data, in a function of added volume of Mal-TIR into ^{15}N MyD88-TIR sample. The best-fit lines to the data, assuming a simple 1:1 complex model, are also shown. Apparent dissociation constants calculated are also indicated with standard errors (see Fig. S3). The black box, red circle, blue triangle, and green triangle indicate the dissociation curves of wild-type, R196A, R288A, and R196A-R288A, respectively.

MyD88-TIR, which lacked the N-terminal death domain and thus was supposedly unable to transmit signals, suppressed LPS-induced luciferase expression. This effect was presumably due to inhibition of signaling pathways by competitive binding of the isolated TIR domain to signaling components that interact with endogenous MyD88. When a TIR mutant harboring a substitution of a functionally important residue is expressed, such suppression is alleviated, which leads to higher LPS-induced luciferase activity than observed with a TIR domain harboring the wild-type sequence. It should be noted that the dominant negative effect of ectopically expressed TIR domain has been used for functional analysis of some key residues of MyD88-TIR in IL-1 signaling (11).

Results from luciferase assays of mutant-expressing cells upon LPS stimulation are shown in Fig. 2*A*. LPS addition to HEK293 cells expressing MD2 and TLR4 resulted in an approximately 3-fold increase in reporter activity, which was consistent with a previous report (18). Alanine substitution of 5 residues, Arg-196, Asp-197, Arg-217, Lys-282, or Arg-288 resulted in significantly reduced inhibitory effects in LPS-induced luciferase activity. Interestingly, these 5 residues are closely associated with the box 1, 2, and 3 motifs, which are highly conserved across TIR domains (see Fig. S1). Arg-196 and Asp-197 are located within the box 2 motif. The side chains of Lys-282 and Arg-288 form a continuous protein surface with box 3 forming residues, and Arg-217 is located distant in the sequence, but proximal in space to the box 1 motif (Fig. 2*B*). Hence, we designated the sites that these residues form as Site II, Site III, and Site I, respectively.

Binding Sites of MyD88-TIR for Mal. Because Site I, Site II, and Site III of the MyD88 TIR domain are important for TLR4-mediated cellular responses following LPS stimulation, the involvement of these sites was examined in direct binding to the TIR domain of Mal (Mal-TIR), the sorting adaptor in MyD88-dependent TLR4 pathways (19). The effect of alanine substitution of Arg-196, Arg-217, or Arg-288 (which forms Site II, Site I, and Site III of the MyD88 TIR domain, respectively) on interactions with Mal-TIR was analyzed by GST pull-down assay. Mal-TIR was pulled down by wild-type MyD88-TIR. However, substitution of either Arg-196 or

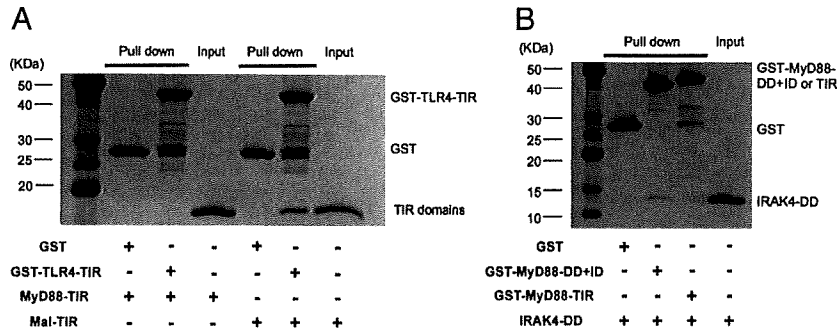

Fig. 3. Direct interactions of MyD88, Mal, TLR4, and IRAK4. (*A*) Binding assay of the TLR4 TIR domain with the MyD88 TIR domain or Mal TIR domain. GST-TLR4-TIR binds Mal-TIR but not MyD88-TIR. (*B*) Binding assay of the IRAK4 death domain with the MyD88 TIR domain or death domain. IRAK4-DD binds the MyD88-DD+ID but not MyD88-TIR.

Arg-288 resulted in moderate, but significant, decreases in MyD88-TIR affinity for Mal-TIR. The MyD88-TIR affinity of the Arg-196 and Arg-288 double-substituted mutant for Mal-TIR was completely abolished (Fig. 2*C*). In contrast, the Arg-217 mutation had no significant effect. The results, therefore, suggested that Site II and Site III, but not Site I, contributed to the interface with Mal-TIR. In addition, Arg-196 substitution by cysteine, which was detected in MyD88 deficiency patients (13), also caused reduced interaction with Mal (Fig. 2*D*). The effect of alanine substitution of those arginine residues on interactions with Mal-TIR was also examined by observing 2D ^{1}H-^{15}N correlation NMR spectra of ^{15}N-labeled MyD88-TIR and its derivative in the absence or presence of various concentrations of nonlabeled Mal-TIR. The ^{15}N-labeled MyD88-TIR signals uniformly decreased upon titration of Mal-TIR (see Fig. S3). Signal attenuation was presumably due to increased apparent molecular weight upon complexation or chemical exchange (Fig. 2*E*). A MyD88-TIR mutation of either Arg-196 or Arg-288 caused moderate effects. However, double mutations of these residues resulted in large effects on signal attenuation, suggesting that signal attenuation was due to interactions between TIR domains of MyD88 and Mal. The apparent dissociation constants were estimated from the signal attenuation of wild-type and mutant MyD88 as previously described (Fig. 2*E*) (20). These results indicated that contributions from Site II and Site III to the interaction were comparable to each other. It should be noted that the effect of tested alanine substitution on the structure of the TIR domain was minor and only limited to the region close to the mutational sites, as judged from the 2D spectra of those mutants. Thus, these substitutions do not affect the opposite functional surface. Therefore, allosteric effect was neglected in interpreting the data.

The Function of Site I in TLR4 Signaling. Site I could serve as an interaction site with cytoplasmic TIR domain of TLR4 (TLR4-TIR), as previously suggested (6). However, an interaction between TIR domains of MyD88 and TLR4 was not detected (Fig. 3*A*). The GST pull-down experiment in the present study further demonstrated that the DD of IRAK4 exhibited no detectable binding activity to MyD88-TIR, but rather bound to MyD88 that lacked the TIR domain (Fig. 3*B*). This indicated that Site I was not involved in interactions with the downstream effector IRAK4, although results from a previous study showed that a small region of TIR, which included box 1 motif, ID, and DD of MyD88, interacts with IRAK4 (21).

Discussion

The TIR domain is typically composed of 135–160 aa residues, with sequence conservation ranging from 20 to 30%. While the hydrophobic core residues are conserved, the surface exposed residues vary greatly between TIR domains. Consequently, the distribution of surface electrostatic potential differs significantly between TIR domains (22), possibly underlying the differences in binding specificity. For TIR domains of membranous receptors, 4 structures from TLR1, TLR2, TLR10, and IL-1RAPL have been reported (8–10). When comparing these, the BB loop of MyD88 displayed the largest structural difference (Fig. 1*C*). The BB loop region has been proposed to be important for interactions between TIR domains. Thus, structural deviation of the BB loop, and differences in surface electrostatic potential, might reflect specificities of TIR–TIR interactions. It should be noted that the isolated MyD88-TIR domain existed as a monomer in solution state, while some TIR domains have been reported to form a dimer in crystal structure (9, 10). On the other hand, full-length MyD88 is known to form a dimer, which seems to be mediated via homomeric interactions between the death domains (see Fig. S2).

The present study identified 3 functional surface sites (Sites I–III) of MyD88-TIR that were important for the LPS-activated TLR4-signaling pathway. Two of these sites, Sites II and III, served as binding sites for Mal-TIR (Fig. 2 *C* and *E*). Results from the GST pull-down and NMR titration experiments suggested that these 2 sites equally contributed to interactions between MyD88-TIR and Mal-TIR. The Site II-forming residues Arg-196 and Asp-197 were located in the BB loop, and were highly conserved across TIR domains (see Fig. S1). Another Mal binding site, Site III, which was formed by 2 basic residues, Lys-282 and Arg-288, flanks the box 3 comprised of FW motif, creating a positively charged surface patch. Because basic amino acids were conserved at positions 282 and 288 (see Fig. S1), this positively charged patch appeared to be common in TIR domains. The present data revealed that Arg-217 in Site I played a crucial role in the TLR4-mediated cellular response to LPS stimulation but was not involved in direct binding to Mal-TIR (Fig. 2*C*). In the GST pull-down experiments, direct interaction of MyD88-TIR with either the TIR domain of TLR4 or the death domain of IRAK4 was not observed (Fig. 3). This was consistent with previous observations that MyD88 does not directly bind to the cytosolic domain of TLR4 (23). Therefore, Site I is unlikely involved in MyD88 interaction with any of the known possible binding partners, such as Mal, TLR4, and IRAK4, but might serve as a contact surface with a yet unidentified MyD88 binding protein or specific membrane portion. The functional role of Site I in TLR4 signaling remains to be clarified in further studies.

The 2 Mal binding sites of MyD88-TIR, Sites II and III, are distantly located from each other and are on opposite molecular surfaces. Thus, it is impossible to assume that one Mal-TIR can make simultaneous contact with both MyD88-TIR sites. In addition, contributions from Site II and Site III to the interaction were shown to be comparable to each other. Thus, assuming 2 Mal-TIR molecules would bind to one MyD88-TIR molecule, we constructed a complex model between MyD88-TIR and Mal-TIR using a molecular docking method similar to previous studies (12, 24). The

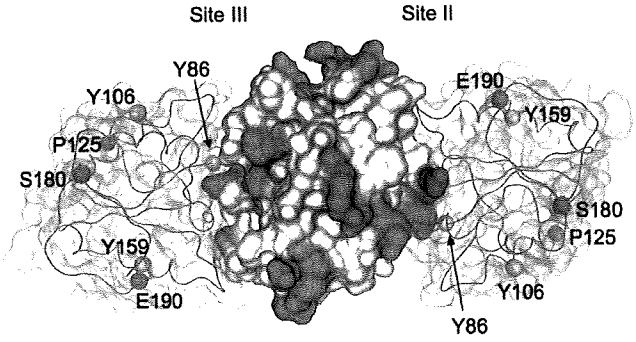

Fig. 4. Structural model of signaling complex formed by MyD88 and Mal. The Mal binding sites, Sites II and III residues, are shown in red, and noncritical residues for signaling and Site I residue are shown in light blue. The positions of the previously reported functional residues (P125, S180, and E190) are shown as orange spheres, and the phosphorylation sites in Mal for signaling, Tyr-86, Tyr 109, and Tyr-159, are shown as yellow spheres.

model indicated that Sites II and III residues are well situated at the interface centers of each Mal-TIR. In addition, all noncritical residues, including Arg-217 (Site I), avoided the interfaces, which supported validity of this model (Fig. 4). Previous reports have shown that P125H mutation or S180L polymorphism of Mal causes decreased interactions between Mal and TLR4 or TLR2, respectively, but has no effect on interactions between Mal and MyD88 (25, 26). Moreover, the TRAF-6 binding site on Mal was shown to include Glu-190 (27). These 3 Mal residues were not included in the Mal-MyD88 complex model interfaces (Fig. 4). Therefore, the model suggested that MyD88-TIR binding might not interfere with interactions between Mal-TIR and TLR4, TLR2, or TRAF-6. Recently, Tyr-86 phosphorylation of Mal was shown to negatively regulate interactions with MyD88 (28). In addition, Tyr-86 mutation, not Tyr-106 or Tyr-159, significantly altered affinity of Mal to MyD88. These observations were consistent with the present complex model, in which Tyr-86, not others, was at the molecular interface (Fig. 4). Moreover, the model predicted that Tyr-86 phosphorylation might perturb MyD88 interface steric complementarity of Mal and result in an electrostatic repulsion to the acidic surface of MyD88-TIR that Mal binds to.

Recently, one of the Site II residues, Arg-196, has just been found to be mutated to cysteine in the new primary immuno-deficiency (MyD88 deficiency) patients (13). This mutation did not cause destabilization of the MyD88 protein, but showed a significant decrease of the direct binding ability between MyD88-TIR and Mal-TIR (Fig. 2*D*). Patients with the MyD88 deficiency were highly susceptible to Gram-positive bacteria, while they showed normal resistance to other kinds of pathogens, such as Gram-negative bacteria and viruses. The phenotypes suggest that TLR2 signaling is more critical than other self-defense systems in early life (3) because the other innate immune signaling pathways have a kind of redundancy, acting as alternative signaling pathways; i.e., TLR2 and TLR4 signaling needs MyD88 and Mal to signal, but TLR4 has other MyD88-independent pathways with TRIF (5). It suggests that the Gram-positive bacterial recognition system is much more dependent on TLR2/MyD88/Mal signaling. The loss of interaction between MyD88 and Mal caused by the mutation would be a critical molecular mechanism for MyD88 deficiency patients.

It is of special interest that the TIR domain of Mal, and not MyD88, directly interacted with the TIR domain of TLR4 (Fig. 3*A*) as described in the previous predicted docking model (29). This observation raises the possibility that Mal-TIR might simultaneously bind to the TIR domains of TLR4 and MyD88, and thereby mediate association as previously predicted (5). Because Mal has been shown to be dispensable for TLR4 signaling when MyD88 is artificially fused to a PIP2 targeting domain (6) there is the possibility that weak interactions between TIR domains of MyD88 and TLR4 mediates signal transduction. Alternatively, an unidentified alternate Mal-independent pathway could contribute to signaling as previously discussed (30). Previous mutation analysis suggests that Mal Pro-125 contributes a binding interface with TLR4 (26). This residue was located distal to the putative MyD88 interface in the present MyD88:Mal complex model and was therefore consistent with the hypothesis that Mal-TIR mediates TIR–TIR interactions between TLR4 and MyD88.

Conclusion

Structure determination combined with functional assays of human MyD88-TIR revealed that 3 sites, which are related to conserved boxes 1–3 of the domain, were important for the LPS/TLR4 pathway. Two of these sites were located at opposite surfaces of the molecule and were shown to mediate direct interaction with Mal-TIR. Thus, the 2 independent binding sites served by MyD88-TIR might contribute to formation of higher order TIR–TIR complexes, which may result in amplification of TLR signal activation. Identification of the key residue in MyD88, which is a direct interacting residue for Mal, is of the clinical significance because one of these residues was shown to be critical for the primary immunodeficiency syndrome. Distribution of the 3 functional sites dispersed on the molecular surface of MyD88-TIR suggested that MyD88 provided multiple interaction surfaces to protein factors that form the signal initiation complex at the cytosolic TLR4 domain. Knowledge of the sites revealed in this study will facilitate further identification of factors and mechanisms used in TLR signaling pathways.

Materials and Methods

Sample Preparation. The portion of the human MyD88 gene encoding the TIR domain (amino acid residues 148–296) was cloned into the vector pGEX-5X-3 (GE Healthcare). This vector was transformed into *Escherichia coli* BL-21 (DE3) (Novagen). The TIR domain of MyD88, which was expressed as a GST (GST) fusion protein, was first purified by glutathione Sepharose 4B FF (GE Healthcare) affinity chromatography, and the GST-tag was removed by digestion with Factor Xa (GE Healthcare). Subsequently, the TIR domain was purified by gel filtration (Sephacryl S-100 HR 26/60 column; GE Healthcare) and cation-exchange chromatography (Mono-S column; GE Healthcare). Using the purification protocol, ^{15}N-labeled, and ^{13}C, ^{15}N-doubly-labeled monomeric TIR domain of MyD88 wild-type proteins were prepared. The protein sample buffer was replaced by 20 mM potassium phosphate buffer (pH 6.0) containing 0.1 mM EDTA and 10 mM DTT. The final protein sample concentration for typical NMR experiments was approximately 0.3 mM.

NMR Spectroscopy. All NMR spectra were recorded at 25 °C on a Bruker DRX500 or DRX800 spectrometer equipped with a cryogenic probe. For assignment of backbone and side chain ^{1}H, ^{13}C, and ^{15}N resonances, a series of triple-resonance experiments were conducted (31). Distance restraints for structure calculations were obtained from 3D ^{15}N-edited NOESY and 3D ^{13}C-edited NOESY experiments, with a mixing time of 150 msec. NMR spectra were processed with NMRPipe software (32) and analyzed using Sparky (33). The pulse sequence used to obtain 2D {^{1}H}-^{15}N steady-state NOE spectra has been previously described (34). The {^{1}H}-^{15}N NOE values were determined from ratios of peak intensities with or without a 3 sec ^{1}H-saturation applied before each scan: NOE = I_{sat}/I_{unsat}.

Structure Calculation. Automated NOESY cross-peak assignment and iterative structure calculation were performed using CYANA version 2.1 (35). The obtained assignment of NOESY cross-peaks was manually validated, and the final structure calculation was performed using CNS version 1.1 (36). Surface electrostatic potentials were calculated using MOLMOL 2K.2 (37).

Cell Culture. Human embryonic kidney (HEK) 293-hTLR4A-HA cells were purchased from Invivogen. These cells were cultured in Dulbecco's modified Eagle's medium (high glucose-containing DMEM, Invitrogen) supplemented with 10% heat-inactivated FBS (Sigma), penicillin (100 U/ml), and streptomycin (100 pg/ml). All cells were incubated at 37 °C in a humidified atmosphere of 5% CO_2.

Vector Preparations. A cDNA encoding the TIR domain (amino acid residues 148–296) that was tagged at the N terminus with a myc-epitope was cloned into

the plasmid vector pcDNA3.1+ (Invitrogen). Mutants of the MyD88 TIR domain were generated using the GeneEditor in vitro Site-Directed Mutagenesis System (Promega). Mutants of each of 25 charged polar amino acid residues (Asp, Glu, Arg, Lys, and His) substituted by alanine were generated. Mutants with poor expression were not included to avoid possible misinterpretation of the loss of dominant negative inhibitory effect. The MD2 construct was also cloned into pcDNA3.1+. A pGL3-Basic Vector (Promega) containing 4 kB binding sites, which was used in the NF-κB luciferase reporter assay, and a Renilla luciferase reporter vector used as an internal control in the assay were gifts from Drs. Sewon Ki and Tetsuro Kokubo (Yokohama City University, Yokohama, Japan).

NF-κB Reporter Gene Activity. 293-hTLR4A-HA cells were transfected with pcDNA3.1+ control vector or pcDNA3.1+ myc-MyD88 TIR domain (wild type or mutant), pcDNA3.1+ MD2, NF-κB luciferase reporter vector, and Renilla luciferase reporter vector, using Lipofectamine 2000 (Invitrogen) according to the manufacturer's instructions. After transfection, the cells were stimulated with LPS O127 (1.0 μg/ml, Sigma) and incubated for 6 hours. Luciferase reporter gene activity was analyzed using the Dual-Luciferase Reporter Assay System (Promega). The inhibitory effect of each TIR mutant expression was assessed in at least 3 independent experiments. The statistical significance of differences in luciferase activities between wild type and mutants in the NF-κB reporter assays was analyzed using Dunnett's multiple comparison test. Statistical significance was assumed to be $P < 0.05$.

GST Pull-Down Assay. The TIR domain of MyD88 wild type and mutants (R196A, R196C, R217A, R288A, and R196A-R288A) was purified as GST-fusion proteins. These expression vectors were generated by subcloning the pcDNA3.1+myc-tagged MyD88 TIR domain into pGEX 5X-1 (GE Healthcare). The DD+ID of MyD88 (amino acid residues 18–141) and TLR4-TIR were also purified as GST-fusion proteins. The GST-fusion proteins were purified by glutathione Sepharose 4B FF (GE Healthcare) affinity chromatography. The TIR domain of human Mal, as well as the DD of IRAK4, was purified using a modified previously reported method (22, 38). These purified proteins were incubated with Glutathione Sepharose 4B (GE Healthcare) for 3 hours. After 4 wash steps with wash buffer (20 mM potassium phosphate buffer (pH 6.0), 100 mM KCl, 0.1 mM EDTA, 10 mM DTT, and 0.5% Triton X-100), the resin was analyzed by SDS polyacrylamide gel electrophoresis and Coomassie Brilliant Blue staining.

NMR Titration. One 15-μl aliquot of 100 μM nonlabeled Mal-TIR was added to 150 μl of 20 μM ^{15}N-labeled MyD88-TIR or its alanine substituted mutants up to 1.5 molar equivalent of ^{15}N MyD88-TIR. At each titration point, 1D ^{1}H-{^{15}N} and 2D ^{1}H-^{15}N SOFAST-HMQC spectra were measured. Quantification of NMR signal attenuation in the titration experiments, and evaluation of apparent dissociation constant (K_d^{app}) for the interaction, are described in *SI Materials and Methods.*

Docking Studies Between MyD88 and Mal. Structure modeling of the TIR domain of Mal was performed using the MyD88-TIR structure as a template on molecular operating environment (MOE) software (39, 40). The docking simulation was performed on AutoDock without any specific restraints between the molecules as previously reported (24, 41, 42). (See detailed method of the docking study in *SI Materials and Methods.*)

ACKNOWLEDGMENTS. We thank Dr. T. Fukao, Dr. H. Kaneko, Dr. Y. Aoki, Dr. H. Morita, Dr. T. Tokumi, W. Souma, and K. Kasahara for their advice and technical help. We thank Dr. S. Ki and Dr. T. Kokubo for their kind gift of vector samples. This work was funded in part by the Research and Development Program for New Bio-industry Initiatives (2005–2009) of the Bio-oriented Technology Research Advancement Institution, Japan. This work was supported by Grants-in-Aid for Scientific Research and the National Project on Protein Structural and Functional Analyses from the Ministry of Education, Science and Culture of Japan. This work was supported by Health and Labour Science Research Grants for Research on Allergic Disease and Immunology from the Ministry of Health, Labour and Welfare.

1. Bonnert TP, et al. (1997) The cloning and characterization of human MyD88: A member of an IL-1 receptor related family. *FEBS Lett* 402:81–84.
2. Kawai T, Akira S (2007) Signaling to NF-kappaB by Toll-like receptors. *Trends Mol Med* 13:460–469.
3. Akira S, Uematsu S, Takeuchi O (2006) Pathogen recognition and innate immunity. *Cell* 124:783–801.
4. Horng T, Barton GM, Flavell RA, Medzhitov R (2002) The adaptor molecule TIRAP provides signalling specificity for Toll-like receptors. *Nature* 420:329–333.
5. O'Neill LA, Bowie AG (2007) The family of five: TIR-domain-containing adaptors in Toll-like receptor signalling. *Nat Rev Immunol* 7:353–364.
6. Kagan JC, Medzhitov R (2006) Phosphoinositide-mediated adaptor recruitment controls Toll-like receptor signaling. *Cell* 125:943–955.
7. Rowe DC, et al. (2006) The myristoylation of TRIF-related adaptor molecule is essential for Toll-like receptor 4 signal transduction. *Proc Natl Acad Sci USA* 103:6299–6304.
8. Xu Y, et al. (2000) Structural basis for signal transduction by the Toll/interleukin-1 receptor domains. *Nature* 408:111–115.
9. Khan JA, Brint EK, O'Neill LA, Tong L (2004) Crystal structure of the Toll/interleukin-1 receptor domain of human IL-1RAPL. *J Biol Chem* 279:31664–31670.
10. Nyman T, et al. (2008) The crystal structure of the human Toll-like receptor 10 cytoplasmic domain reveals a putative signalingd. *J Biol Chem* 283:11861–11865.
11. Li C, Zienkiewicz J, Hawiger J (2005) Interactive sites in the MyD88 Toll/interleukin (IL) 1 receptor domain responsible for coupling to the IL1beta signaling pathway. *J Biol Chem* 280:26152–26159.
12. Jiang Z, et al. (2006) Details of Toll-like receptor:adapter interaction revealed by germ-line mutagenesis. *Proc Natl Acad Sci USA* 103:10961–10966.
13. von Bernuth H, et al. (2008) Pyogenic bacterial infections in humans with MyD88 deficiency. *Science* 321:691–696.
14. Burns K, et al. (1998) MyD88, an adapter protein involved in interleukin-1 signaling. *J Biol Chem* 273:12203–12209.
15. Slack JL, et al. (2000) Identification of two major sites in the type I interleukin-1 receptor cytoplasmic region responsible for coupling to pro-inflammatory signaling pathways. *J Biol Chem* 275:4670–4678.
16. Poltorak A, et al. (1998) Defective LPS signaling in C3H/HeJ and C57BL/10ScCr mice: Mutations in Tlr4 gene. *Science* 282:2085–2088.
17. Adachi O, et al. (1998) Targeted disruption of the MyD88 gene results in loss of IL-1- and IL-18-mediated function. *Immunity* 9:143–150.
18. Shimazu R, et al. (1999) MD-2, a molecule that confers lipopolysaccharide responsiveness on Toll-like receptor 4. *J Exp Med* 189:1777–1782.
19. Kagan JC, et al. (2008) TRAM couples endocytosis of Toll-like receptor 4 to the induction of interferon-beta. *Nat Immunol* 9:361–368.
20. Lu J, Chen M, Dekoster GT, Cistola DP, Li E (2008) The RXRalpha C-terminus T462 is a NMR sensor for coactivator peptide binding. *Biochem Biophys Res Commun* 366:932–937.
21. Burns K, et al. (2003) Inhibition of interleukin 1 receptor/Toll-like receptor signaling through the alternatively spliced, short form of MyD88 is due to its failure to recruit IRAK-4. *J Exp Med* 197:263–268.
22. Dunne A, Ejdeback M, Ludidi PL, O'Neill LA, Gay NJ (2003) Structural complementarity of Toll/interleukin-1 receptor domains in Toll-like receptors and the adaptors Mal and MyD88. *J Biol Chem* 278:41443–41451.
23. Brown V, Brown RA, Ozinsky A, Hesselberth JR, Fields S (2006) Binding specificity of Toll-like receptor cytoplasmic domains. *Eur J Immunol* 36:742–753.
24. Kato Z, et al. (2008) Positioning of autoimmune TCR-Ob. 2F3 and TCR-Ob. 3D1 on the MBP85–99/HLA-DR2 complex. *Proc Natl Acad Sci USA* 105:15523–15528.
25. Khor CC, et al. (2007) A Mal functional variant is associated with protection against invasive pneumococcal disease, bacteremia, malaria and tuberculosis. *Nat Genet* 39:523–528.
26. Horng T, Barton GM, Medzhitov R (2001) TIRAP: An adapter molecule in the Toll signaling pathway. *Nat Immunol* 2:835–841.
27. Mansell A, Brint E, Gould JA, O'Neill LA, Hertzog PJ (2004) Mal interacts with tumor necrosis factor receptor-associated factor (TRAF)-6 to mediate NF-kappaB activation by toll-like receptor (TLR)-2 and TLR4. *J Biol Chem* 279:37227–37230.
28. Piao W, et al. (2008) Tyrosine phosphorylation of MyD88 adapter-like (Mal) is critical for signal transduction and blocked in endotoxin tolerance. *J Biol Chem* 283:3109–3119.
29. Nunez Miguel R, et al. (2007) A dimer of the Toll-like receptor 4 cytoplasmic domain provides a specific scaffold for the recruitment of signalling adaptor proteins. *PLoS ONE* 2:e788.
30. Monie TP, Moncrieffe MC, Gay NJ (2009) Structure and regulation of cytoplasmic adapter proteins involved in innate immune signaling. *Immunol Rev* 227:161–175.
31. John C, Wayne JF, Arthur GIP, Rance M, Nicholas JS (2007) *Protein NMR Spectroscopy: Principles And Practice* (Academic, San Diego), 2nd Ed.
32. Delaglio F, et al. (1995) NMRPipe: A multidimensional spectral processing system based on UNIX pipes. *J Biomol NMR* 6:277–293.
33. Goddard TD, Kneller DG (1999) SPARKY 3 (University of California, San Francisco).
34. Farrow NA, et al. (1994) Backbone dynamics of a free and a phosphopeptide-complexed Src homology-2 domain studied by N-15 Nmr relaxation. *Biochemistry* 33:5984–6003.
35. Guntert P (2004) Automated NMR structure calculation with CYANA. *Methods Mol Biol* 278:353–378.
36. Brunger AT, et al. (1998) Crystallography & NMR system: A new software suite for macromolecular structure determination. *Acta Crystallogr D* 54:905–921.
37. Koradi R, Billeter M, Wuthrich K (1996) MOLMOL: A program for display and analysis of macromolecular structures. *J Mol Graphics 14:51-* 55:29–32.
38. Lasker MV, Gajjar MM, Nair SK (2005) Cutting edge: Molecular structure of the IL-1R-associated kinase-4 death domain and its implications for TLR signaling. *J Immunol* 175:4175–4179.
39. Levitt M (1992) Accurate modeling of protein conformation by automatic segment matching. *J Mol Biol* 226:507–533.
40. Fechteler T, Dengler U, Schomburg D (1995) Prediction of protein three-dimensional structures in insertion and deletion regions: A procedure for searching data bases of representative protein fragments using geometric scoring criteria. *J Mol Biol* 253:114–131.
41. Stoddard BL, Koshland DE, Jr (1992) Prediction of the structure of a receptor-protein complex using a binary docking method. *Nature* 358:774–776.
42. Morris GM, Goodsell DS, Huey R, Olson AJ (1996) Distributed automated docking of flexible ligands to proteins: Parallel applications of AutoDock 2.4. *J Comput Aided Mol Des* 10:293–304.

Allergology International. 2009;58:111-117
DOI: 10.2332/allergolint.O-08-549

ORIGINAL ARTICLE

Various Expression Patterns of α1 and α2 Genes in IgA Deficiency

Hiroko Suzuki[1], Hideo Kaneko[1], Toshiyuki Fukao[1], Rong Jin[1], Norio Kawamoto[1], Tsutomu Asano[1], Eiko Matsui[1], Kimiko Kasahara[1] and Naomi Kondo[1]

ABSTRACT

Background: IgA deficiency (IgAD) is the most common immunodeficiency, however the pathogenesis in most cases of IgAD is unknown. There are 2 subclasses of IgA, IgA1 and IgA2, and its heavy chains are encoded by 2 different genes, the α1 and α2 genes. To investigate the molecular pathogenesis of IgA deficiency, it is important to evaluate each of the expressions of IgA1 and IgA2 separately.

Methods: In this study, we report on the reverse transcriptase (RT)-PCR method in which α1 and α2 mRNAs can be separately evaluated. This method is based on electrophoretic separation using the difference of 39 bases between α1 and α2 mRNAs. Three selective, 5 partial and 2 secondary IgAD patients were examined.

Results: In the 3 selective IgAD patients, no α1 or α2 mRNA expression was detected. In the 5 partial IgAD patients, various α1 and α2 mRNA expression patterns were found. One of the partial IgAD patients showed only α2 gene expression, but not α1 gene expression, and was found to show an α1 gene deletion together with γ2 and ε gene deletions. His plasma IgA2 level was within the normal range.

Conclusions: Patients with an α1 gene deletion can be considered as having partial IgAD. Using this method, we identified the second case of α1 gene deletion in Japan, and classified IgAD patients on the basis of α1 and α2 expression.

KEY WORDS

gene expression, IgA subclasses, partial IgA deficiency, selective IgA deficiency, α1 gene deletion

ABBREVIATIONS

IgA, immunoglobulin A; IgAD, immunoglobulin A deficiency; RT, reverse transcriptase; CVID, common variable immunodeficiency; TACI, transmembrane activator and calcium-modulator and cyclophilin ligand interactor; SD, standard deviation; PBMCs, peripheral blood mononuclear cells; GAPDH, glyceraldehyde-3-phosphate dehydrogenase; ELISA, enzyme-linked immunosorbent assay; HRP, horseradish peroxidase; BSA, bovine serum albumin; PBS, phosphate-buffered saline

INTRODUCTION

Human immunoglobulin A (IgA) is the most abundant immunoglobulin in secretions. IgA has 2 subclasses, IgA1 and IgA2. The ratios of IgA1 : IgA2 are approximately 9 : 1 in serum and 6 : 4 in saliva.[1] In mucosal tissue, IgA synthesis greatly exceeds that of other immunoglobulin classes. These 2 subclasses play important roles in the first line of defense, and the amount ratio of these molecules in secretions varies.

Selective IgA deficiency (IgAD) is the most common immunodeficiency, and has been found with a frequency ranging from 0.03 to 0.3%. The prevalence differs according to ethnic groups, with a lower frequency in the Japanese population, namely, 1/18,000 people.[2,3] Most IgAD patients remain healthy, but some suffer from a variety of infections, allergies, autoimmune disorders, gastrointestinal diseases, malignancies, endocrinopathies, neurological diseases, and genetic disorders.[2,4] The pathogenesis of IgAD has not yet been completely clarified. IgAD has been found to be associated with IgG2, IgG4, and IgE deficiencies.[5-8] The class switch disorder in IgA-producing B lymphocytes is one of the most important factors in IgAD patients.[9] Asano *et al.* suggested

[1]Department of Pediatrics, Graduate School of Medicine, Gifu University, Gifu, Japan.
Correspondence: Hiroko Suzuki, Department of Pediatrics, Graduate School of Medicine, Gifu University, 1-1 Yanagido, Gifu 501-1194, Japan.
Email: hori_hiro2002@yahoo.co.jp
Received 11 March 2008. Accepted for publication 29 July 2008.

Table 1 Immunological data of patients

Patient No.	Sex	Age	Serum level (mg/dl)			IgG subclass (mg/dl)			
			IgG	IgA	IgM	IgG1	IgG2	IgG3	IgG4
Selective IgA deficiency									
1	M	10 years	1363	< 5	146	619	255	57.3	33.9
2	F	11 years	1640	< 5	117	949	400	47.7	90.2
3	F	17 years	1261	< 5	137	630	625	35.1	18.4
Partial IgA deficiency									
4	M	4 years	1223	17	120	933	< 8.0	22.8	< 3.0
5	F	3 years	1644	15	150	878	47.9	17.3	32.1
6	F	3 years	869	27	106	306	69.3	27.6	3.8
7	M	4 years	887	45	101	295	97.0	40.0	4.4
8	M	4 years	1624	8	100	1090	120	74.7	< 3.0
Secondary IgA deficiency									
9	F	7 years	913	12	105	602	148	52.8	16.5
10	M	13 years	705	9	39	852	345	49.8	6.4

that decreased expression levels of Iα germline transcripts before a class switch may be the cause of selective IgAD, and B-cell differentiation might be disturbed after a class switch in partial IgAD patients.[10] Husain *et al.* reported that the increased destruction of a subset of B cells is the cause for the inability to produce IgA in IgAD patients.[11]

The association between IgAD and common variable immunodeficiency (CVID) has been discussed,[3] and it was reported recently that some CVID and IgAD patients have mutations in TNFRSF13B (encoding TACI; transmembrane activator and calcium-modulator and cyclophilin ligand interactor).[12,13]

The molecular weights of the IgA1 and IgA2 heavy chains are both approximately 53 kD. The α1 and α2 genes show about 97% of its identity.[14] This high homology between them makes it difficult to analyze the α1 and α2 genes separately. The α-chain constant region of both α1 and α2 genes is encoded by 3 exons. The hinge region of the human α chain is encoded at the beginning of the second exon. The hinge region of the α2 gene shows a deletion of 39 nucleotides (corresponding to 13 amino acids) when compared with that of the α1 gene.[1,15] To clarify the pathogenesis and immunological reactions of IgAD clear, we analyzed α1 and α2 gene expression in IgAD patients. In this study, we devised a new method to determine the expression levels of the α1 and α2 genes, and analyzed selective, partial and secondary IgAD patients.

METHODS

SUBJECTS

As shown in Table 1, we analyzed 3 selective IgAD patients (patients number 1, 2 and 3) with serum IgA levels below the detection limit (<5 mg/dl), 5 partial IgAD patients (patients number 4, 5, 6, 7, and 8) with serum IgA levels above 5 mg/dl but having more than 2 standard deviations (SDs) below the normal level, and 2 secondary IgAD patients (patients number 9 and 10) whose conditions were caused by epileptic medication. Ten controls were also included in this study. Two of the 10 controls were child volunteers under 16 years of age, and the other 8 were adult volunteers 16 years or older. We obtained informed consent from the patients, controls, and parents of minors.

CELL PREPARATION

Peripheral blood mononuclear cells (PBMCs) were collected in heparin and separated by gradient centrifugation in Ficoll-Paque (GE Healthcare Bio-Sciences AB, Uppsala, Sweden).[16] The cells were suspended at a density of 10^6/ml and incubated for 24 hours in RPMI 1640 medium supplemented with 10% heat-inactivated fetal calf serum, 2 mmol/l l-glutamine, 100 U/ml penicillin and 100 μg/ml streptomycin.[10] In comparison with non-cultured cells, cells cultured for 24 hours showed higher levels of α1 and α2 gene expression (unpublished data).

cDNA SYNTHESIS AND PCR AMPLIFICATION

We extracted total RNA from PBMCs using an Isogen kit (Nippon Gene, Tokyo, Japan), and cDNA synthesis was carried out using 1 or 2 μg of total RNA with oligo-dT and M-MLV reverse transcriptase (Invitrogen, Carlsbad, CA, USA). We used the following PCR primer pair, which was targeted to the common sequence area of the α1 and α2 genes: sense 5'-CCTGGTCACCGTCTCCTCA-3' (placed at the J exon; Gene Bank accession number-L20778) and antisense 5'-TCACGCTCAGGTGGTCCTTG-3' (placed at the Cα CH2 exon)[17] (Fig. 1A). The PCR fragments included the CH1, hinge and CH2 regions, and the size was 532 bp for the α1 gene and 493 bp for the α2 gene. The PCR program was 35 or 40 cycles of 94℃

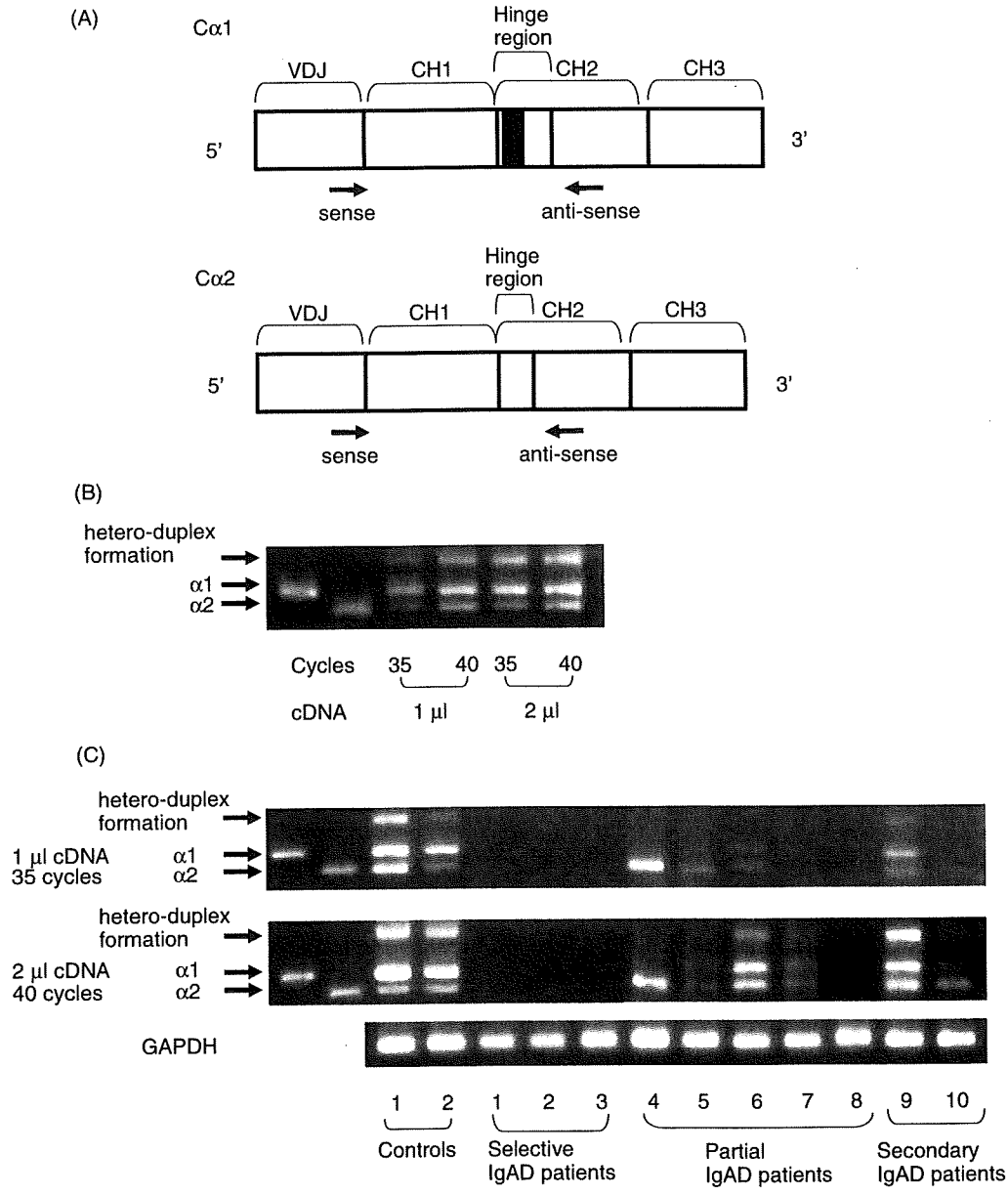

Fig. 1 Structure and expression of the α1 and α2 genes. (**A**) The primer pair was targeted to the common sequence area of the α1 and α2 genes. These figures show mature Cα gene transcripts. The arrows indicate the positions of the primers. The black box indicates the deletion of 39 bases. VDJ: variable diversity joining region, CH: constant heavy chain. (**B**) RT-PCR analysis of RNA extracted from the PBMCs of a control subject, starting from 1 μl or 2 μl of cDNA and using 35 or 40 cycles. The two lanes at the left show PCR products amplified from the template DNA, which are T-vectors containing the IgA1 (lane 1) or IgA2 (lane 2) genes. (**C**) RT-PCR analysis of RNA extracted from the PBMCs of control subjects and IgAD patients. The α1 fragment, α2 fragment, and hetero-duplex formation are indicated by arrows. GAPDH was used as a control.

for 1 minute, 60℃ for 1 minute, and 72℃ for 1 minute using 1 or 2 μl of cDNA. The PCR products were run on 4% agarose gels for 120 minutes. Glyceraldehyde-3-phosphate dehydrogenase (GAPDH) was used as a control.

DNA EXTRACTION AND PCR AMPLIFICATION

Genomic DNA was purified from polymorphonuclear

cells using Sepa Gene (Sanko Junyaku, Tokyo, Japan). We used the following PCR primer pair, which was targeted at the common sequence area of the α1 and α2 genes: sense 5'-TGACCAGCTCAGGCCATCT CT-3' and antisense 5'-CTTTGCAAACCAGAGCACT GA-3'. The PCR program was 40 cycles of 94℃ for 1 minute, 58℃ for 1 minute, and 72℃ for 1 minute. Four percent agarose gel electrophoresis was performed for 120 minutes. The other primer pairs were as follows: for amplification of the Cε gene, sense 5'-A CCTTCAGCGGTAAGAGAGGG-3' and antisense 5'-T GGGAACGTACCTGCACACTT-3', (the PCR program was 35 cycles of 94℃ for 1 minute, 60℃ for 1 minute, and 72℃ for 1 minute); for amplification of the Cγ2 gene, sense 5'-ATCTCTTCCTCAGCACCACCT-3' and antisense 5'-CGTGGCACTCATTTACCCGGA-3', (the PCR program was 35 cycles of 94℃ for 1 minute, 58 ℃ for 1 minute, and 72℃ for 1 minute); for the Cμ gene, sense 5'-ATGTGTGTCCCCGGTGAGTGA-3' and antisense 5'-AGGGCCACCCCTGTGAACAGA-3', (the PCR program was 35 cycles of 94℃ for 1 minute, 58℃ for 1 minute, and 72℃ for 1 minute).

QUANTIFICATION OF IgA SUBCLASSES IN PLASMA

The levels of the IgA subclasses in plasma were measured by enzyme-linked immunosorbent assay (ELISA). For IgA1, coating was performed with a mouse monoclonal anti-IgA1 (NI69-11), and detection of IgA1 was performed with horseradish peroxidase (HRP)-labeled goat anti-human IgA (Cappel, Organon Teknika, Turnhout, Belgium).[18] For IgA2, coating was performed using goat anti-human IgA (BETHYL, Montgomery, TX, USA), and detection of IgA2 was performed using mouse anti-human IgA2-HRP (B3506B4).[19] ELISA plates were coated overnight at 4 ℃ with mouse monoclonal anti-IgA1 (diluted to 1 : 200 with 0.05 M sodium carbonate, pH 9.6) or goat anti-human IgA (diluted to 1 : 100 with 0.05 M sodium carbonate, pH 9.6). The plates were washed then incubated with standard serum and plasma dilutions. IgA1 was detected using goat anti-human IgA-HRP (diluted to 1 : 10000 with 1% bovine serum albumin [BSA] in phosphate-buffered saline [PBS]-0.02% Tween 20), and IgA2 was detected using mouse anti-human IgA2-HRP (diluted to 1 : 1000 with 1% BSA in PBS-0.02% Tween 20). The samples were tested repeatedly. The lower limits of IgA1 and IgA2 detection were 5 ng/ml and 1 μg/ml, respectively.

RESULTS

PCR AMPLIFICATION OF α1 AND α2 GENE EXPRESSION

RT-PCR analysis was performed using primer pairs that amplified both α1 and α2 mRNAs and could distinguish α2 mRNA from α1 mRNA taking advantage of the deletion of 39 bases in the hinge region of the α2 gene. Various PCR conditions were tested, and the optimal conditions were deemed to be 2 μl of cDNA and 40 cycles of amplification (Fig. 1B). Control samples gave an intense α1 band and a less-intense, shorter α2 band in all 4 PCR conditions. Another band with less electrophoretic mobility than the α1 band was determined to be a hetero-duplex formation of the α1 and α2 fragments, because the subcloning of this band yielded clones of the α1 and α2 fragments. Figure 1C shows α1 and α2 gene expression in 10 IgAD patients. In 3 selective IgAD patients (patients number 1, 2 and 3), no expression of the α1 and α2 genes was detected. Three partial IgAD patients (patients number 5, 6 and 7) and 2 secondary IgAD patients (patients number 9 and 10) showed α2 and α1 gene expressions; however, patient No. 4 showed only α2 gene expression, but no α1 gene expression. One partial IgAD patient (No. 8) showed no bands in this RT-PCR analysis.

PLASMA IgA LEVELS IN CONTROLS AND IgAD PATIENTS

Plasma IgA1 and IgA2 levels were assayed separately (Table 2). The IgA1 levels were much higher than the IgA2 levels in the 10 controls. In the 3 selective IgAD patients, plasma IgA1 and IgA2 levels were very low. One partial IgAD patient (patient No. 4) had a normal IgA2 level, but no detectable IgA1. This finding is in accordance with the result of this patient showing no α1 gene expression in PBMCs. Although the IgA2 level of patient No. 5 was below the threshold, other patients with partial IgAD (patients number 6, 7, 8) showed various IgA1 and IgA2 levels although these levels were much lower than that of the control group.

PCR AMPLIFICATION OF THE IMMUNOGLOBULIN GENES OF IgAD PATIENTS

In patient No. 4, α1 gene expression was not detected and no IgA1 protein was detected in his plasma. As shown in Table 1, the plasma levels of the IgG subclasses showed that IgG2 and IgG4 levels were below the detection limits. Hence, we carried out PCR amplification of the genomic α2 and α1 genes, together with the μ, γ2 and ε genes. As shown in Figure 2, no PCR products were detected for the α1, γ2 and ε genes in patient No. 4, whereas they were clearly be detected in 2 control and other IgAD patients. A large genomic deletion of the A1-GP-G2-G4-E genes can be proposed as the molecular basis of IgAD in patient No. 4.

LONGITUDINAL CHANGE IN THE SERUM IgA LEVEL OF PATIENT NO. 4

The immunological data of 2 families of patients with IgG2-IgG4-IgA1-IgE deficiency, including patient No. 4, are shown in Table 3. The serum IgA levels of patient No. 4 over time are shown in Table 4. The patient's IgA levels remained at a level more than 2 SDs

Table 2 The levels of IgA subclasses and IgA1/IgA2 ratios in plasma as measured by ELISA

Patient No.	Serum IgA levels (mg/dl)	Plasma IgA1 and IgA2 levels (mg/dl)		IgA1/IgA2 ratio	mRNA expression		Genes	
		IgA1	IgA2		α1	α2	α1	α2
Selective IgA deficiency								
1	< 5	2.48 ± 0.26	ND†	NC‡	−¶	−	+§	+
2	< 5	ND	ND	NC	−	−	+	+
3	< 5	2.16 ± 0.74	ND	NC	−	−	+	+
Partial IgA deficiency								
4	17	ND	13.67 ± 1.39	NC	−	+	−	+
5	15	2.71 ± 0.36	ND	NC	+	+	+	+
6	27	8.28 ± 0.52	0.91 ± 0.25	8.40	+	+	+	+
7	45	29.29 ± 6.83	4.88 ± 0.54	6.97	+	+	+	+
8	8	6.28 ± 0.67	0.86 ± 0.45	8.87	−	−	+	+
Secondary IgA deficiency								
9	12	8.59 ± 1.77	1.17 ± 0.36	6.56	+	+	+	+
10	9	0.56 ± 0.09	0.18 ± 0.03	3.03	+	+	+	+
Controls ($n = 10$)		128.02 ± 36.98	19.39 ± 8.93	7.96 ± 4.14				

† ND : undetected, ‡ NC : not calculated.
§ + : detected, ¶ − : undetected.

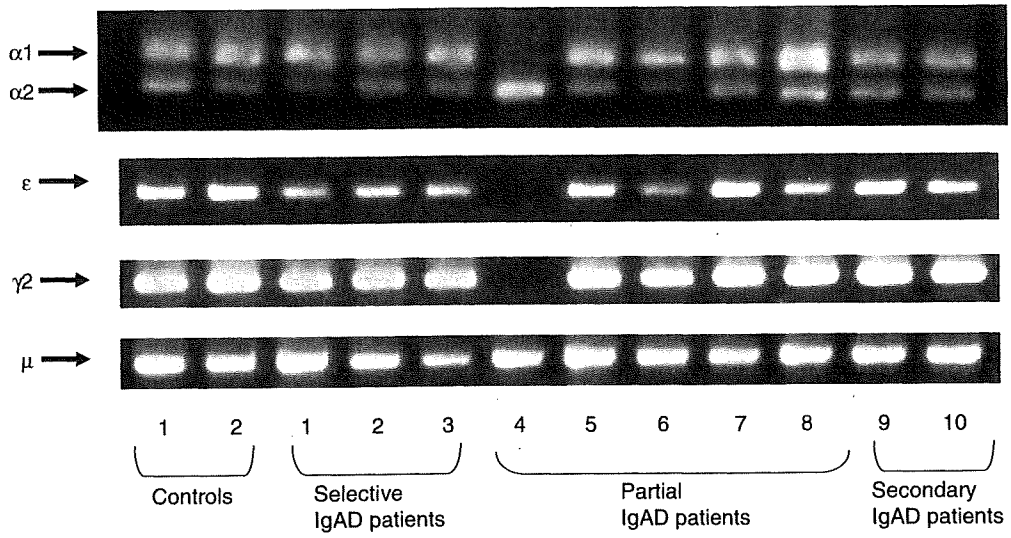

Fig. 2 PCR analysis of immunoglobulin genes in IgAD patients. PCR analysis of α1, α2, ε, γ2 and μ genes was performed in control subjects and IgAD patients. Two different sized bands for the α gene appeared, corresponding to the α1 and α2 genes, as indicated by arrows.

below the normal value, but above 5 mg/dl. The immunological data of his family members are shown in Family 1 (Table 3). The patient's older brother was also found to have the same gene deletion. His serum IgA level was 21 mg/dl, and he also showed a pattern of partial IgAD. The serum IgA levels of another patient with IgG2-IgG4-IgA1-IgE deficiency and her family members are shown as Family 2 (Table 3).[8] Both the patient and her older sister had the same deletions of the A1-GP-G2-G4-E genes. The serum IgA level of the patient's sister was 18 mg/dl and she also showed a pattern of partial IgAD.

DISCUSSION

The serum IgA subclass levels of IgAD patients, particularly selective IgAD patients, are very difficult to measure by ELISA; thus, there have been few reports on the levels of serum IgA subclasses in IgAD patients. The α1 and α2 gene expression levels are low in most IgAD patients, and there have been no previous reports on the gene expression levels of the IgA subclasses in these patients.[20-23] Hummelshoj *et al.*

Table 3 Immunological data of patient no. 4 and 2 families of patients with IgG2-IgG4-IgA1-IgE deficiency

Family 1							
	Age	Serum level					
		mg/dl					IU/ml
		IgA	IgG1	IgG2	IgG3	IgG4	IgE
Patient No. 4	4	17	933	< 8.0	22.8	< 3.0	< 2.0
Father	45	119	659	451	58.0	19.0	70.0
Mother	41	201	730	224	25.4	14.2	190.0
Brother	11	21	952	< 8.0	23.3	< 3.0	< 2.0
Family 2							
	Age	Serum level					
		mg/dl					IU/ml
		IgA	IgG1	IgG2	IgG3	IgG4	IgE
Patient	1	< 5	996	< 8.0	10.4	< 3.0	< 5.0
Father	27	161	720	281	13.7	14.1	214.8
Mother	26	180	794	248	16.7	8.2	4.2
Sister	3	18	645	< 8.0	15.1	< 3.0	< 5.0

Table 4 Longitudinal change in the serum IgA levels of patient no. 4

	20m	25m	30m	38m	56m	57m
Serum IgA level (mg/dl)	11	12	11	11	20	17
Normal value†	1year	2y		3y	4y	
Mean (±2SD)	49 (16−128)	60 (20−149)		74 (25−174)	89 (31−202)	

† data on normal values according to reference 28.

reported on the expression of germline transcripts of the α1 and α2 genes in IgAD patients.[24] The germline transcripts were induced during stimulation with TGF-β, however their levels were lower than those of control subjects. Our report shows the expression of mature transcripts of the α1 and α2 genes in partial IgAD patients. In the 3 selective IgAD patients, no expression of α1 and α2 genes was detected, presumably because the expression level was too low. In 2 of them, only plasma IgA1 levels could be measured, and in 1 of them, neither IgA1 nor IgA2 levels were unable to be measured. Patient No. 8 showed no mRNA expression of IgA subclasses, but exhibited detectable levels of plasma IgA1 and IgA2 levels. It might be assumed that the pathogenesis of partial IgAD in patient No. 8 is similar to that in selective IgAD patients. As shown in Table 2, patients number 1, 2, 3 and 8 showed no α1 or α2 gene expression, while patients number 5, 6, 7, 9 and 10 showed both α1 and α2 gene expression. There is a possibility that the mechanism underlying IgA deficiency may be different between these 2 groups. The plasma IgA2 levels were unable to be measured in 1 partial IgAD patient; however, α2 gene expression was seen in this patient using our method. This method is effective for determining whether partial IgAD patients lack expression of the α1 and α2 genes when their plasma IgA, IgA1 and IgA2 levels are under the detection limit.

Asano *et al.* reported detectable levels of the Cα mature transcripts by RT-PCR using the same sense primer we employed and an antisense primer located in the Cα CH1 region.[10] Using our method, no α1 or α2 gene expression was detected in 3 selective IgAD patients. There was a difference in the annealing temperatures used (59℃ in the study of Asano *et al.*), and different PCR conditions may result due to changes in the sensitivity of the assay.

IgAD patients are often associated with IgG subclass deficiency. In our study, 2 IgAD patients (patients number 4 and 8) had IgG subclass deficiency in the serum. Patient No. 4 showed deletions of the γ2 and ε genes, and was considered to have a large genomic deletion of the Cα1, ΨCγ, Cγ2, Cγ4 and Cε genes, showing the same observations reported previously in a patient.[8] In Japan, only 1 case has ever been reported. Beard *et al.*[25] reported that IgA-IgG2-IgG4 deficiency occurs in 4% of 73 IgAD patients. Deletions of the A1-GP-G2-G4-E genes are the most common deletions of the Ig heavy chain locus.[26] There could be more patients with an α1 gene deletion who might have partial IgAD. Partial IgAD is

often transient,[27] however, patients who have a deletion of the α gene will not show transient IgAD and will exhibit continuous partial IgAD.

We also classified the IgAD patients on the basis of the expression of α1 and α2 genes. Selective IgAD patients showed no α1 or α2 mRNA expression and extremely low protein levels, while secondary IgAD patients showed both mRNA and protein expressions of IgA subclasses. Partial IgAD can be classified into 3 patterns as follows: cases showing reduced levels of α1 and α2 gene expression; cases showing no α1 gene expression but normal α2 gene expression; and cases showing no α1 or α2 gene expression.

It is sometimes difficult to determine the pathogenic mechanisms operative in IgAD patients on the basis of serum IgA levels. Variations in the pathogenesis of IgAD patients might become better understood by examining the protein and mRNA expression levels of IgA subclasses.

ACKNOWLEDGEMENTS

This study was partly supported by a grant from the Ministry of Health, Labour and Welfare of Japan.

REFERENCES

1. Kerr MA. The structure and function of human IgA. *Biochem J* 1990;**271**:285-96.
2. Cunningham-Rundles C. Physiology of IgA and IgA deficiency. *J Clin Immunol* 2001;**21**:303-9.
3. Hammarstrom L, Vorechovsky I, Webster D. Selective IgA deficiency and common variable immunodeficiency. *Clin Exp Immunol* 2000;**120**:225-31.
4. Schaffer FM, Monteiro RC, Volanakis JE, Cooper MD. IgA deficiency. *Immunodefic Rev* 1991;**3**:15-44.
5. Bottaro A, de Marchi M, de Lange GG, Carbonara AO. Gene deletions in the human immunoglobulin heavy chain constant region gene cluster. *Exp Clin Immunogenet* 1989;**6**:55-9.
6. Lefranc MP, Hammarstrom L, Smith CI, Lefranc G. Gene deletions in the human immunoglobulin heavy chain constant region locus: molecular and immunological analysis. *Immunodefic Rev* 1991;**2**:265-81.
7. Plebani A, Carbonara AO, Bottaro A *et al.* Gene deletion as cause of associated deficiency of IgA1, IgG2, IgG4 and IgE. *Immunodeficiency* 1993;**4**:245-8.
8. Terada T, Kaneko H, Li AL *et al.* Analysis of Ig subclass deficiency: First reported case of IgG2, IgG4, and IgA deficiency caused by deletion of Cα1, ΨCγ, Cγ2, Cγ4 and Cε in a Mongoloid patient. *J Allergy Clin Immunol* 2001;**108**: 602-6.
9. Islam KB, Baskin B, Nilsson L, Hammarstrom L, Sideras P, Smith CI. Molecular analysis of IgA deficiency. *J Immunol* 1994;**152**:1442-52.
10. Asano T, Kaneko H, Terada T *et al.* Molecular analysis of B-cell differentiation in selective or partial IgA deficiency. *Clin Exp Immunol* 2004;**136**:284-90.
11. Husain Z, Holodick N, Day C, Szvmanski I, Alper CA. Increased apoptosis of $CD20^+IgA^+B$ cells is the basis for IgA deficiency: The molecular mechanism for correction in vivo by IL-10 and CD40L. *J Clin Immunol* 2006;**26**:113-25.
12. Salzer U, Chapel HM, Webster ADB *et al.* Mutations in TNFRSF13B encoding TACI are associated with common variable immunodeficiency in humans. *Nat Genet* 2005; **37**:820-8.
13. Castigli E, Wilson SA, Garibyan L *et al.* TACI is mutant in common variable immunodeficiency and IgA deficiency. *Nat Genet* 2005;**37**:829-34.
14. Flanagan JG, Lefranc MP, Rabbitts TH. Mechanisms of divergence and convergence of the human immunoglobulin alpha 1 and alpha 2 constant region gene sequences. *Cell* 1984;**36**:681-8.
15. Chintalacharuvu KR, Raines M, Morrison SL. Divergence of human α-chain constant region gene sequences. *J Immunol* 1994;**152**:5299-304.
16. Kondo N, Fukutomi O, Agata H *et al.* The role of T lymphocytes in patients with food-sensitive atopic dermatitis. *J Allergy Clin Immunol* 1993;**91**:658-68.
17. Stavnezer J. Immunoglobulin class switching. *Curr Opini Immunol* 1996;**8**:199-205.
18. Klasen IS, Goertz JH, van de Wiel GA, Weemaes CM, van der Meer JW, Drenth JP. Hyper-immunoglobulin A in the hyperimmunoglobulinemia D syndrome. *Clin Diagn Lab Immunol* 2001;**8**:58-61.
19. Camacho MT, Outschoorn I, Echevarria C *et al.* Distribution of IgA subclass response to *Coxiella burnetii* in patients with acute and chronic Q fever. *Clin Immunol Immunopathol* 1998;**88**:80-3.
20. Park SR, Kim HA, Chun SK, Park JB, Kim PH. Mechanisms underlying the effects of LPS and activation-induced cytidine deaminase on IgA isotype expression. *Mol Cells* 2005;**19**:445-51.
21. Islam KB, Nilsson L, Sideras P, Hammarstrom L, Smith CI. TGF beta-1 induces germ-line transcripts of both IgA subclasses in human B lymphocytes. *Int Immunol* 1991;**3**: 1099-106.
22. Nilsson L, Islam KB, Olafsson O *et al.* Structure of TGF-beta 1-induced human immunogloblin C alpha 1 and alpha 2 germ-line transcripts. *Int Immunol* 1991;**3**:1107-15.
23. Kitani A, Strober W. Differential regulation of Cα1 and Cα2 germ-line and mature mRNA transcripts in human peripheral blood B cells. *J Immunol* 1994;**153**:1466-77.
24. Hummelshoj L, Ryder LP, Nielsen LK, Nielsen CH, Poulsen LK. Class switch recombination in selective IgA-deficient subjects. *Clin Exp Immunol* 2006;**144**:458-66.
25. Beard LJ, Ferrante A. IgG4 deficiency in IgA-deficient patients. *Pediatr Infect Dis J* 1989;**8**:705-9.
26. Brusco A, Saviozzi S, Cinque F, Bottaro A, DeMarchi M. A recurrent breakpoint in the most common deletion of the Ig heavy chain locus (del A1-GP-G2-G4-E). *J Immunol* 1999;**163**:4392-8.
27. Plebani A, Ugazio AG, Monafo V, Burgio GR. Clinical heterogeneity and reversibility of selective immunoglobulin A deficiency in 80 children. *Lancet* 1986;**1**:829-31.
28. Kawai T, Iida Y, Kojima Y *et al. [Normal value of laboratory examination in Japanese pediatric practice].* Tokyo: Japan Public Health Association, 1996 (in Japanese).

ELSEVIER

Cancer Genetics and Cytogenetics 192 (2009) 86–89

Cancer Genetics and Cytogenetics

Short communication

Translocation (1;10)(p34;p15) in infant acute myeloid leukemia with extramedullary infiltration in multiple sites

Michinori Funato*, Toshiyuki Fukao, Hideo Sasai, Tomohiro Hori, Daisuke Terazawa, Michio Ozeki, Kenji Orii, Takahide Teramoto, Hideo Kaneko, Naomi Kondo

Department of Pediatrics, Graduate School of Medicine, Gifu University, Yanagido 1-1, Gifu 501-1194, Japan

Received 23 February 2009; accepted 9 April 2009

Abstract Primary acute myeloid leukemia (AML) with extramedullary infiltration (EMI) in multiple sites is rare. Herein, we describe a case of infant AML with EMI in multiple sites. She had dyspnea and hypofibrinogenemia at diagnosis, and systemic computed tomography revealed EMI in the orbit, gingiva, bronchial pathway, and urinary tract. Bone marrow examination confirmed the diagnosis of AML with t(1;10)(p34;p15). No case of AML with t(1;10)(p34;p15) has been reported in the literature. At the present time, she remains free of disease 12 months after bone marrow transplantation (BMT) in the second complete remission.

1. Introduction

Extramedullary infiltration (EMI) includes tumor nodules (myeloid or granulocytic sarcoma), skin infiltration (leukemia cutis), meningeal infiltration, gingival infiltration, or hepatosplenomegaly [1]. The incidence of primary acute myeloid leukemia (AML) with EMI is reported to be between 7 and 49% among pediatric AML patients [1–3]. Moreover, most patients have isolated or double infiltration sites, and primary AML with EMI in multiple sites is rare, reportedly 0.1–4% of pediatric AML patients [1–4].

Herein, we describe a case of infant AML with EMI in multiple sites, namely in the orbit, gingiva, bronchial pathway, and urinary tract. Cytogenetic analysis of bone marrow cells revealed a 46,XX,t(1;10)(p34;p15) karyotype. This is the first report to describe the occurrence of AML with t(1;10)(p34;p15). At present, she has survived without recurrence of the disease for 12 months since bone marrow transplantation (BMT) from a histocompatibility locus antigen (HLA)-matched donor in the second complete remission (CR).

2. Materials and methods

2.1. Case report

A 7-month-old girl was referred to Gifu University Hospital because of mild elevations of liver enzymes with a 1-month history of congestion and poor weight gain. Physical examination and hematological data on admission were unremarkable, except for a slight increase in serum level of aspartate transaminase of 99U/liter, alanine transaminase of 62 U/liter, and lactate dehydrogenase of 504 U/liter. We tentatively diagnosed her as having mild elevations of liver enzymes as a result of viral infection.

Eight days after admission, hoarseness and a bulging appearance of the eyelids and gingiva became evident (Fig. 1). Blood examination showed a decrease in fibrinogen to below 50 mg/dL, without immature cells in the peripheral blood smear. In addition, computed tomography of the total body revealed the presence of an infiltrating mass lesion in the left urinary tract, an infiltrating orbital lesion, and mild enlargement of the liver (Fig. 2). A bone marrow examination then confirmed the diagnosis of AML (FAB M4; Fig. 3A). Flow cytometric immunophenotyping in the blast cells was positive for CD15, CD33, CD34, CD64, and CD65. No leukemia cells were detected in the cerebral spinal fluid.

On the 11th hospital day, chemotherapy, according to the Japan Association of Childhood Leukemia Study (JACLS) AML99 protocol, consisting of etoposide (VP16), cytosine arabinoside, mitoxantrone, and idarubicin, was started. On the same day, she developed dyspnea and needed mechanical ventilation support for 7 days. Two months later, she achieved CR and received four courses of chemotherapy according to the JACLS AML99 protocol as consolidation.

However, she relapsed 4 months later. A bone marrow examination revealed the same myeloblasts. After she

* Corresponding author. Tel.: +81-58-2306386; fax: +81-58-2306387.
E-mail address: mfunato@mac.com (M. Funato).

0165-4608/09/$ – see front matter
doi:10.1016/j.cancergencyto.2009.04.010

Allergology International. 2009;58:97-102
DOI: 10.2332/allergolint.O-07-530

ORIGINAL ARTICLE

Age-Related Changes of Transforming Growth Factor β1 in Japanese Children

Masahiro Morimoto[1], Eiko Matsui[1], Norio Kawamoto[1], Satomi Sakurai[1], Hideo Kaneko[1], Toshiyuki Fukao[1], Shinichi Iwasa[2], Makoto Shiraki[2], Kimiko Kasahara[1] and Naomi Kondo[1]

ABSTRACT

Background: Transforming growth factor β1 (TGFβ1) is an important factor in immunomodulation. The expression of TGFβ1 has been shown to be influenced by the C-509T polymorphism in the TGFβ1 gene. We investigated age-related changes of plasma TGFβ1 levels in a birth-cohort study. In addition, the genotypes of the C-509T polymorphism were investigated in allergic and non-allergic subjects.

Methods: Sixty-four neonates who met the following criteria were enrolled in this cohort study: 1) full-term vaginally delivery; 2) underwent DNA polymorphism analysis; and 3) questionnaire forms were filled out by parents at 0, 6 and 14 months of age. The umbilical cord blood at 0 months and peripheral blood at 6, and 14 months were collected. Plasma TGFβ1 levels were measured at 0, 6 and 14 months of age. Genomic DNA was extracted from their umbilical cord blood. The genotype of the subjects was examined for the presence of C-509T.

Results: The plasma TGFβ1 level at 6 months was the highest of the 3 measurements (at 0, 6, and 14 months of age). The TGFβ1 levels at 14 months in allergic subjects were significantly higher than those in non-allergic subjects (p = 0.03). All subjects with bronchial asthma (n = 3) had the TT genotype of the C-509T polymorphism.

Conclusions: The plasma TGFβ1 levels change with age. In addition, TGFβ1 may play a role in the pathogenesis of bronchial asthma.

KEY WORDS

bronchial asthma, single nucleotide polymorphism (SNP), transforming growth factorβ1 (TGFβ1), umbilical cord blood

INTRODUCTION

Transforming growth factorβ1 (TGFβ1) is a 25 kDa disulfide-linked homodimeric multifunctional cytokine. TGFβ1 may be the most important growth factor related to immunomodulatory effects because knockout mice died of massive inflammatory lesions.[1] The role of TGFβ1 in allergic diseases have been reported.[2-4] The levels of TGFβ1 concentration were found to be higher in the bronchoalveolar lavage fluid of patients with asthma compared with subjects without asthma.[3] The expression of TGFβ1 was found to be influenced by polymorphisms in the TGFβ1 gene, some of which may be associated with bronchial asthma and other diseases.[4,5] In particular, the T allele of the C-509T polymorphism within the TGFβ1 gene was associated with elevated serum TGFβ1 levels and also associated with elevated levels of total IgE in allergic asthma patients.[5,6]

In this study, we investigated the age-related changes of TGFβ1 levels in a birth-cohort study. In addition, C-509T within the TGFβ1 gene in subjects with asthma was compared with non-allergic subjects.

METHODS

SUBJECTS

Sixty-four neonates born at Iwasa Maternity Hospital in Gifu Prefecture between November 2005 and July

[1]Department of Pediatrics, Graduate School of Medicine, Gifu University and [2]Iwasa Maternity Hospital, Gifu, Japan.
Correspondence: Eiko Matsui, MD, PhD, Department of Pediatrics, Gifu University Graduate School of Medicine, 1-1 Yanagido, Gifu 501-1193, Japan.
Email: eikom@gifu-u.ac.jp
Received 3 December 2007. Accepted for publication 22 July 2008.

Table 1 Characteristics of subjects

Gender	Male	32	Female	32
Birth body weight (g)	Mean±SD	3137.1 ± 400.5 (range: 2410–4026g)		
Gestational week	Mean±SD	39w3d ± 1w2d (range: 37w6d–41w1d)		
Family history of allergy	Father	With allergy 25		
		Without allergy 32		
		No record 7		
	Mother	With allergy 34		
		Without allergy 24		
		No record 6		
Family smoking history with 1 or both parents still smoking	Present	16	Absent	48

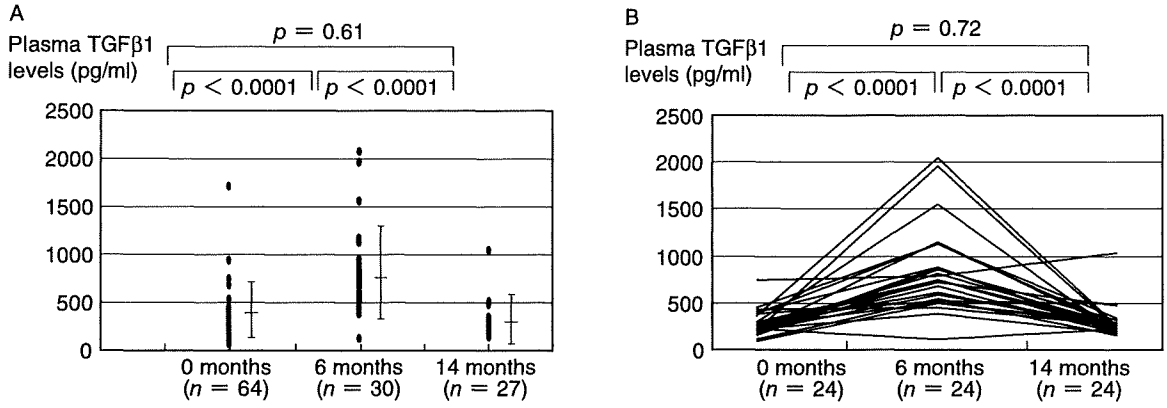

Fig. 1 (**A**) Plasma TGFβ1 levels at 0, 6, and 14 months of age. (**B**) Changes of plasma TGFβ1 levels in 24 subjects whose data were available at all three points.

2006, and satisfying the following criteria were enrolled in this cohort study: 1) full-term vaginally delivery; 2) underwent DNA polymorphism analysis; and 3) questionnaire forms were filled out by parents at 0, 6 and 14 months of age. Informed consent, including DNA analysis, was obtained from the parents of the neonates during their stay in the hospital. This cohort study was approved by the Ethical Committee of the Graduate School of Medicine of Gifu University. Umbilical cord blood samples were collected from 64 neonates and peripheral blood samples were also collected for analysis from 30 subjects at 6 months and from 27 subjects at 14 months of age. Subjects who were given a diagnosis of atopic dermatitis and bronchial asthma during the follow-up over a period of 14 months after birth, were classified as having those diseases. Allergic subjects were defined as those who were given a diagnosis of atopic dermatitis and/or bronchial asthma and non-allergic subjects were defined as those having neither atopic dermatitis nor bronchial asthma during the 14-month observation period. Some data of the recruited population are summarized in Table 1.

ASSAYS FOR PLASMA IgE LEVELS AND PLASMA TGFβ1 LEVELS

Plasma samples obtained from heparinized blood were kept at -30℃. Plasma IgE levels were determined by chemiluminescent enzyme immunoassay and plasma TGFβ1 levels were measured with a human ELISA kit (R & D Systems, Mineapolis, MN, USA); the detection range was 31.2–2000 pg/ml.

DETECTION OF C-509T WITHIN THE TGFβ1 GENE

Genomic DNA was extracted from the heparinized umbilical cord blood using a Sepagene kit (Sanko Junyaku, Tokyo, Japan). The TGFβ1 gene was amplified and sequenced using the PCR technique and an ABI 3100 DNA sequencer (Applied Biosystems, Foster City, CA, USA). The primers used for amplification of the DNA fragments were the forward primer at position -737– -718 (5'-CAGACTCTAGAGACTGTC AG-3') and the reverse primer at position -320– -338 (5'-GTCACCAGAGAAAGAGGAC-3').

STATISTICAL ANALYSES

The relations between age and plasma in TGFβ1 lev-